The multi-layer multi-configuration time-dependent Hartree method for bosons: Theory, implementation, and applications

Lushuai Cao, Sven Krönke, Oriol Vendrell, and Peter Schmelcher

Citation: The Journal of Chemical Physics **139**, 134103 (2013); doi: 10.1063/1.4821350
View online: http://dx.doi.org/10.1063/1.4821350
View Table of Contents: http://scitation.aip.org/content/aip/journal/jcp/139/13?ver=pdfcov
Published by the AIP Publishing

The multi-layer multi-configuration time-dependent Hartree method for bosons: Theory, implementation, and applications

Lushuai Cao,[1,2,a),b)] Sven Krönke,[1,a),c)] Oriol Vendrell,[2,3,d)] and Peter Schmelcher[1,2,e)]
[1]*Zentrum für Optische Quantentechnologien, Universität Hamburg, Luruper Chaussee 149, D-22761 Hamburg, Germany*
[2]*The Hamburg Centre for Ultrafast Imaging, Luruper Chaussee 149, D-22761 Hamburg, Germany*
[3]*Center for Free-Electron Laser Science, DESY, Notkestrasse 85, D-22607 Hamburg, Germany*

(Received 7 June 2013; accepted 2 September 2013; published online 1 October 2013)

We develop the multi-layer multi-configuration time-dependent Hartree method for bosons (ML-MCTDHB), a variational numerically exact *ab initio* method for studying the quantum dynamics and stationary properties of general bosonic systems. ML-MCTDHB takes advantage of the permutation symmetry of identical bosons, which allows for investigations of the quantum dynamics from few to many-body systems. Moreover, the multi-layer feature enables ML-MCTDHB to describe mixed bosonic systems consisting of arbitrary many species. Multi-dimensional as well as mixed-dimensional systems can be accurately and efficiently simulated via the multi-layer expansion scheme. We provide a detailed account of the underlying theory and the corresponding implementation. We also demonstrate the superior performance by applying the method to the tunneling dynamics of bosonic ensembles in a one-dimensional double well potential, where a single-species bosonic ensemble of various correlation strengths and a weakly interacting two-species bosonic ensemble are considered. © *2013 AIP Publishing LLC*. [http://dx.doi.org/10.1063/1.4821350]

I. INTRODUCTION

The numerical simulation of the quantum dynamics of strongly correlated many-body systems is a topic of widespread and pronounced interest. Such simulations represent a tough task in general due to the exponential scaling of the state space: taking an interacting N-particle system, for example, and allowing each particle to occupy M single particle states, the many-body Hilbert space turns out to be M^N dimensional for a system of distinguishable particles. When going to higher particle numbers, one, hence, has to truncate the Hilbert space in one or another way. Moreover, this scaling problem has serious consequences for the simulation of the dynamics: In the course of time, the system state will move through different subspaces of the total Hilbert space in general. If one now tries to expand the systems state with respect to a time-independent basis, many basis states will be needed in order to span the relevant subspace for the whole propagation time. So for reducing the number of basis vectors, one should better employ a time-dependent, moving basis, in which the instantaneous system state can be optimally represented.

In the multi-configuration time-dependent Hartree method (MCTDH), such a co-moving basis is provided by time-dependent Hartree products.[1,2] The equations of motion for the single particle functions (SPFs) building up the time-dependent Hartree products as well as for the expansion coefficients are obtained by means of the Dirac-Frenkel variation principle, which ensures a variationally optimal representation of the total wave function at any instant. Using Hartree products as the many-body basis states, MCTDH is well suited for dealing with distinguishable particles. Originally developed in the context of quantum molecular dynamics, MCTDH has successfully been applied to an enormous diversity of problems concerning the vibrational and wave packet dynamics of molecules (cf. Refs. 3 and 4 and reference therein). Moreover, MCTDH also turned out to be powerful for simulating strongly correlated few-body systems of ultracold, indistinguishable bosonic atoms in traps, see, e.g., Refs. 5 and 6.

MCTDH has been extended for dealing with higher particle numbers in several ways: In multi-layer MCTDH (ML-MCTDH), degrees of freedom (DOF) are combined to higher-dimensional ones. The MCTDH expansion scheme is then applied to these combined modes and their constituting degrees of freedom in a cascade.[7,8] This scheme is particularly fruitful for scenarios where there are strong correlations within certain subsystems while the inter-subsystem correlations are relatively weak.[9] Especially, many system-bath problems are of this type. In such a situation, the necessary number of time-dependent basis functions can be reduced by combining the strongly correlated degrees of freedom in a ML-MCTDH expansion. As MCTDH, ML-MCTDH is based on expansions in terms of Hartree products and, thus, ignores possible particle exchange symmetries of the system. When considering an interacting bosonic bath, the resulting redundancies in the configuration space limit the feasible numbers of the indistinguishable degrees of freedom and SPFs.

[a)]L. Cao and S. Krönke have contributed equally to this work.
[b)]lcao@physnet.uni-hamburg.de
[c)]Sven.Kroenke@physnet.uni-hamburg.de
[d)]oriol.vendrell@cfel.de
[e)]pschmelc@physnet.uni-hamburg.de

In contrast to this, the MCTDH method for fermions (MCTDHF) and for bosons (MCTDHB) reduce the number of expansion coefficients by expanding the total wave function in terms of slater determinants and permanents,[10–13] respectively. MCTDHF has been applied in the context of quantum chemistry as well as for molecules in strong laser fields.[14–17] The crossover from the Gross-Pitaevskii to the many-body regime has been studied for several ultracold bosonic systems by means of MCTDHB (see Refs. 18 and 19 and the references therein). There is even a formalism, which unifies MCTDHB and MCTDHF for dealing, e.g., with bose-bose, bose-fermi, and fermi-fermi mixtures.[20,21] Furthermore, an extension for considering particle conversion, i.e., chemical reactions, in a multi-species system has been developed.[22]

ML-MCTDH features a high flexibility with respect to the wave function expansion: Any way of combining degrees of freedom to higher dimensional ones in a cascade is allowed and leads to a specific wave function *Ansatz*. As, in the case of indistinguishable particles, many of these mode-combination schemes do not reflect the indistinguishability of the particles, the particle exchange (anti-) symmetry can, in general, not be incorporated in ML-MCTDH, making ML-MCTDH incompatible with MCTDHB and MCTDHF. There is, however, an exception: In Ref. 23, a second quantization representation of ML-MCTDH (ML-MCTDH-SQR) has been derived, which has been applied to charge transport problems,[24,25] for example. The ML-MCTDH-SQR method is based on the factorization of the Fock space for m single particle modes into m sub-Fock spaces corresponding to just one single particle mode each, which leads to the product structure required by ML-MCTDH. By the virtue of this product structure, the m modes can be identified with the "lower dimensional" DOF of a ML-MCTDH setting and any mode combination of these DOF to higher dimensional DOF in a cascade becomes possible. In this way, ML-MCTDH-SQR benefits from the flexible cascade scheme of ML-MCTDH while keeping the SPF, constituting the Fock states, time-independent.

In this work, an alternative symbiosis employing the bosonic symmetry and a multi-layer *Ansatz* is presented, in which the SPFs of the bosons are time-dependent. The price one has to pay for this is that only two expansion schemes (and any combination thereof) are possible: (i) a multi-layer expansion with respect to the different bosonic species for optimally taking account inter- and intra-species correlations and (ii) a particle multi-layer expansion in which the single particle functions are further expanded in the MCTDH form for efficiently simulating bosons in two- and three-dimensional traps. This method, termed multi-layer MCTDHB (ML-MCTDHB), manifests itself as a numerically exact *ab initio* tool for the quantum dynamics as well as stationary properties of bosonic ensembles consisting of arbitrary many species in various dimensions. This paper is devoted to the detailed derivation of the underlying theory, the description of the implementation, as well as the account of algorithmic features of the method. While Ref. 26 contains a brief account of the theory of ML-MCTDHB and focuses on its applications to the nonequilibrium quantum dynamics of mixtures of ultracold atoms, the present work provides the complete theoretical framework necessary for the reader to thoroughly understand and apply the theory. Furthermore, we provide relevant technical aspects, address the strategy of an efficient implementation, and demonstrate the efficiency of ML-MCTDHB by comparing the number of expansion coefficients with the existing methods such as MCTDHB for bose-bose mixtures by applying it to some relevant example systems.

This paper is organized as follows: in Sec. II, we introduce two different schemes of ML-MCTDHB, the species ML-MCTDHB (in Sec. II A) and the particle ML-MCTDHB (in Sec. II B), which are for bosonic mixtures and bosonic systems in high dimensions, respectively. The combination of these two schemes leading to the general ML-MCTDHB theory is then introduced in Sec. II C. In Secs. II D and II E, we comment on the scaling property and the symmetry preservation of ML-MCTDHB, respectively. In Sec. III, we discuss some details of the implementation of the method, including the implementation of the second quantization scheme (Sec. III A) and the applicabilities of the method (Sec. III B). In Sec. IV, the application of ML-MCTDHB is illustrated by two examples. We conclude with a summary, discussing also an extension of ML-MCTDHB to fermionic species in Sec. V.

II. THEORY

A. ML-MCTDHB for bosonic mixtures

1. Hamiltonian and Ansatz

ML-MCTDHB is designed for the most general bosonic mixtures containing an arbitrary number of bosonic species, with all possible types of single particle potentials for each species as well as intra-/inter-species interaction potentials. The bosonic species can refer to different bosonic quasi-particles, chemical species, isotopes, or atoms of the same element prepared in different hyperfine bosonic states, which have been widely realized in experiments.[27–29] ML-MCTDHB can treat bosons with various DOF, including one- to three-dimensional spatial DOF as well as spatial plus internal (e.g., the spinor) DOF. The Hamiltonian of such bosonic mixtures can be expressed in the general form of

$$\hat{H} = \sum_{\kappa}\sum_{i}\hat{H}^0_{\kappa}(i) + \sum_{\kappa}\sum_{i<j}\hat{V}_{\kappa}(i,j) + \sum_{\kappa_1<\kappa_2}\sum_{i_{\kappa_1},j_{\kappa_2}}\hat{W}_{\kappa_1,\kappa_2}(i_{\kappa_1},j_{\kappa_2}). \quad (1)$$

The first term of the Hamiltonian contains the single particle Hamiltonian for all the bosons in each species with $\hat{H}^0_{\kappa} = \hat{T}_{\kappa} + \hat{U}_{\kappa}$, and $\hat{T}_{\kappa}$ as well as $\hat{U}_{\kappa}$ refer to the kinetic energy and single particle potentials of the κ species bosons, respectively. Particularly $\hat{U}_{\kappa}$ can be a spatial potential and also a spin-orbit coupling potential for bosons with spin DOF. The second and third terms of Eq. (1) are the intra- and inter-species interactions. The intra-/inter-species interactions, $\hat{V}_{\kappa}$ and $\hat{W}_{\kappa_1,\kappa_2}$, respectively, can be of arbitrary form such as the contact interaction, the dipolar interaction, or the Coulomb interaction, which are widely studied in various physics and chemistry fields. In this work, the interactions are restricted to the two-body interactions. Moreover,

since ML-MCTDHB is a variational *ab initio* method for the time-dependent Schrödinger equation, all the potentials can be time-dependent in ML-MCTDHB.

ML-MCTDHB applies a multi-layer *Ansatz* for a bosonic mixture of arbitrary many species. To introduce the multi-layer *Ansatz*, we consider a general bosonic mixture containing S species, and bosons of each species evolve in a fixed single particle Hilbert space, which is spanned by a set of time-independent basis functions, e.g., $\{|r_j^\kappa\rangle\}_{j=1}^{\mathcal{M}_\kappa}$ for the bosons of species κ, which we call κ bosons for brevity in the following. The Hilbert space of the total system is chosen as the direct product of a given Hilbert space of each species, as $\mathcal{H} = \prod_{\kappa=1}^{S} \mathcal{H}^\kappa$, where $\mathcal{H}$ and $\mathcal{H}^\kappa$ refer to the Hilbert space of the total system and the κ species, respectively. Consequently, the total wave vector $|\Psi\rangle$ of the system, temporally evolving in $\mathcal{H}$, is expanded in Hartree products of the vectors in each $\mathcal{H}^\kappa$, as

$$|\Psi\rangle = \sum_{i_1=1}^{M_1} \cdots \sum_{i_S=1}^{M_S} A^1_{i_1,\ldots,i_S} \prod_{\kappa=1}^{S} |\phi^{2;\kappa}_{i_\kappa}\rangle. \tag{2}$$

$|\phi^{2;\kappa}_{i_\kappa}\rangle$ refers to a vector in $\mathcal{H}^\kappa$, and $A^1_{i_1,\ldots,i_S}$ is the time-dependent expansion coefficient. For simplicity, we omit all time-dependencies in the notation in this paper.

In ML-MCTDHB, $\{|\phi^{2;\kappa}_i\rangle\}|_{i=1}^{M_\kappa}$ for all species, i.e., $\kappa \in [1, S]$, are set to be time-dependent, and they are evolving within the corresponding Hilbert space $\mathcal{H}^\kappa$. Instead of taking the basis vectors of $\mathcal{H}^\kappa$ as the direct product of $|r^\kappa\rangle$ of all the κ bosons, a set of time-dependent SPFs $\{|\phi^{3;\kappa}_i\rangle\}|_{i=1}^{m_\kappa}$ is assigned to each of the κ bosons, and the basis vectors of $\mathcal{H}^\kappa$ are then chosen as the permanent states with respect to $\{|\phi^{3;\kappa}_i\rangle\}|_{i=1}^{m_\kappa}$ in the second quantization picture, as

$$|\vec{n}_\kappa\rangle = (N_\kappa! n_1! \ldots n_{m_\kappa}!)^{-\frac{1}{2}} \sum_{\pi \in S(N_\kappa)} \left|\phi^{3;\kappa}_{i_{\pi(1)}}\right\rangle_1 \ldots \left|\phi^{3;\kappa}_{i_{\pi(N_\kappa)}}\right\rangle_{N_\kappa}. \tag{3}$$

$|\vec{n}_\kappa\rangle = |(n_1, \ldots, n_{m_\kappa})\rangle$ is the permanent state, with n_i the boson number in the state $|\phi^{3;\kappa}_i\rangle$, and $|\phi^{3;\kappa}_i\rangle_j$ denotes that the jth κ boson is in the state $|\phi^{3;\kappa}_i\rangle$. The summation runs over all permutations π of the first N_κ integers, i.e., $\pi : [1, N_\kappa] \to [1, N_\kappa]$. $\mathcal{H}^\kappa$ is then spanned by the basis vectors of $\{|\vec{n}_\kappa\rangle\}$, and $|\phi^{2;\kappa}_{i_\kappa}\rangle$ is expanded as

$$\left|\phi^{2;\kappa}_i\right\rangle = \sum_{\vec{n}_\kappa | N_\kappa} A^{2;\kappa}_{i;\vec{n}_\kappa} |\vec{n}_\kappa\rangle. \tag{4}$$

The notation $\vec{n}_\kappa | N_\kappa$ indicates the constraint that the occupation numbers n_i have to sum up to the number of κ bosons, i.e., N_κ.

The SPFs, $\{|\phi^{3;\kappa}_i\rangle\}|_{i=1}^{m_\kappa}$, are in turn evolving in the single particle Hilbert space spanned by the time-independent basis $\{|r_j^\kappa\rangle\}_{j=1}^{\mathcal{M}_\kappa}$, as

$$\left|\phi^{3;\kappa}_i\right\rangle = \sum_{j=1}^{\mathcal{M}_\kappa} A^{3;\kappa}_{i;j} \left|r^\kappa_j\right\rangle. \tag{5}$$

Please note that the expansion scheme (2)–(5) is based on a cascade of truncations. Having the number of time-independent basis states $\mathcal{M}_\kappa$ fixed, one may consider any number of single particle functions $m_\kappa = 1, \ldots, \mathcal{M}_\kappa$ and any number of species states $M_\kappa = 1, \ldots, \binom{N_\kappa + m_\kappa - 1}{m_\kappa - 1}$, so that m_κ and M_κ serve as numerical control parameters for simulating bosonic ensembles of different intra- and inter-species correlations.

The combination of Eqs. (2)–(5) complete the cascade expansion of the system wave vector $|\Psi\rangle$ with respect to the fixed basis $\{|r_\kappa\rangle\}$, and a concept of multi-layer structure can be identified: $|\Psi\rangle$ corresponds to the top layer and $\{|\phi^{2;\kappa}_i\rangle\}$, $\{|\phi^{3;\kappa}_i\rangle\}$ form the species and particle layer, respectively. $\{|r_\kappa\rangle\}$ are related to the physical or in accordance with the MCTDH terminology[2] primitive DOF, e.g., the spatial and internal DOF, while $\{|\phi^{2;\kappa}_i\rangle\}$ and $\{|\phi^{3;\kappa}_i\rangle\}$ are related to the so-called logical DOF on the species and particle layers, respectively. Each logical DOF on the species layer represents one bosonic species, and each logical DOF on the particle layer represents a boson of the corresponding species. In the following, $\{|r_\kappa\rangle\}$ are termed as the primitive basis, with $\{|\phi^{3;\kappa}_i\rangle\}$ and $\{|\phi^{2;\kappa}_i\rangle\}$ named as the particle and species SPFs of corresponding logical DOF of related layers. The class of wave function decomposition is denoted as the *species multi-layer MCTDHB Ansatz*.

In practice, $|r^\kappa\rangle$ can be taken as the state of one boson locating at position r^κ in space, and this choice of the primitive basis vectors $|r^\kappa\rangle$ can naturally cover high-dimensional systems. Consider, for instance, the κ bosons possessing three-dimensional spatial DOF plus one spin DOF, i.e., $r^\kappa = (x^\kappa, y^\kappa, z^\kappa, s^\kappa)$, then the vector $|r^\kappa\rangle$ is seen as the product $|x^\kappa\rangle|y^\kappa\rangle|z^\kappa\rangle|s^\kappa\rangle$, denoting one boson located at spatial position $(x^\kappa, y^\kappa, z^\kappa)$ and in spin state s^κ. We refer to such a treatment of higher dimensional SPFs $|\phi^{3;\kappa}_i\rangle$ by means of a product basis of one-dimensional time-independent basis states as primitive mode combination. A more efficient treatment of high-dimensional systems with ML-MCTDHB will be introduced in Sec. II B.

Let us summarize the species ML-MCTDHB with the introduction of the tree diagram notation, in analogy to Ref. 8. An example of the tree structure is shown in Figure 1, for which we consider a three-species bosonic mixture containing the bosonic species A, B, and C. The primitive basis of A and B bosons is spanned with respect to a single spatial DOF $\{x^A\}$ and $\{x^B\}$, respectively, with the DOF of the y- and z-dimension frozen out by strong confinement potentials, while the C bosons are in three-dimensional space denoted by (x^C, y^C, z^C). The tree diagram is composed of various nodes and links connecting the nodes. The nodes in the tree refer to the primitive as well as logical DOF, and the links indicate the expansion relation between corresponding DOF. In Figure 1, the top node refers to the state vector of the whole system $|\Psi\rangle$, and it forms the top layer of the tree. The second layer is the species layer formed by the species nodes, and each species node corresponds to the logical DOF of one bosonic species associated with the species SPFs $\{|\phi^{2;\kappa}_i\rangle\}$ ($\kappa = A, B, C$). One layer below, i.e., the third layer, is the particle layer, of which each node refers to a particle logical DOF with the particle SPFs $\{|\phi^{3;\kappa}_i\rangle\}$. The nodes below the particle nodes relate to the primitive spatial DOF, which are indicated inside boxes. It now becomes clear that a circle node refers to a logical DOF associated with time-dependent basis vectors, and a square

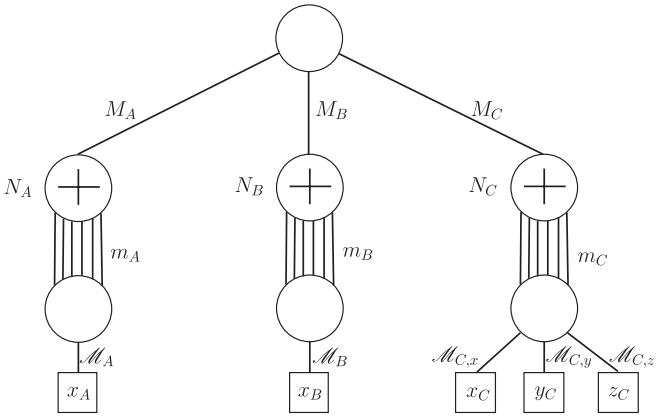

FIG. 1. The tree diagram of a three-species bosonic system. The three species are labeled as A, B, and C bosons, with primitive DOF of x_A, x_B, and (x_C, y_C, z_C), respectively. Corresponding to the ML-MCTDHB *Ansatz*, a three-layer tree diagram is shown, containing the top layer, the species layer, the particle layer from top to bottom. The nodes on each non-top layer correspond to different logical DOF, and the primitive DOF are given by the square nodes at the bottom. The "+" inside the species nodes denotes the species to be a bosonic species.

refers to a primitive DOF associated with time-independent basis vectors. The links between nodes in adjacent layers refer to the expansions given in Eqs. (2)–(5), for instance, the three branches leading out of the top node correspond to the expansion of $|\Psi\rangle$ by Eq. (2). Particularly, the multiple vertical lines linking the species and particle nodes indicate that the species node represents a logical DOF to which many bosons rather than a single one are combined. The number given along each link denotes the number of SPFs or primitive vectors of the node at the bottom side of the link. Moreover, the "+" sign in the species node indicates the related node as a logical DOF of a bosonic species, and the number on the left side of each species node indicates the number of bosons of this species. In this way, the tree diagram offers the complete information of the ML-MCTDHB *Ansatz*, in a visualized manner, and the superscripts of the SPFs and expansion coefficients, $|\phi_i^{\alpha;\kappa}\rangle$ and $A_{i;I}^{\alpha;\kappa}$ indicate that the corresponding DOF is the κth node on the αth layer.

2. Derivation and general form of the equations of motion for the expansion coefficients

In this section, we derive the equations of motion for the coefficients of the ML-MCTDHB *Ansatz* (2)–(5) for a general mixture containing S bosonic species, of which the Hamiltonian is given by Eq. (1) and the time-independent primitive basis of each species is chosen as $\{|r_j^\kappa\rangle\}_{j=1}^{\mathscr{M}_\kappa}$.

The time propagation of the system (both in real and imaginary time) is given by the time evolution of all the coefficients in the *Ansatz*, which can be derived from the Dirac-Frenkel variational principle[30–32]

$$\langle \delta\Psi | (i\partial_t - \hat{H}) | \Psi \rangle = 0. \tag{6}$$

Here, we adapt the natural units and set $\hbar = 1$. For all Ansatz considered in this work, the Dirac-Frenkel variational principle turns out to be equivalent to the Lagrangian and to the McLachlan's principle.[32–34] The latter essentially says: Propagate your *Ansatz* $|\Psi\rangle$ according to $i\partial_t|\Psi\rangle = |\Theta\rangle$ with $|\Theta\rangle$ minimizing $|||\Theta\rangle - \hat{H}|\Psi\rangle||^2$. This ensures that we obtain a variationally optimal wave function within our class of *Ansätzes*.

To calculate $|\delta\Psi\rangle$ and $i\partial_t|\Psi\rangle$ in (6), we first introduce a new expression of the permanent state as

$$|\vec{n}_\kappa\rangle = \sum_i \sqrt{\frac{n_i}{N_\kappa}} \left|\phi_i^{3;\kappa}\right\rangle_1 |\vec{n}_\kappa - \hat{i}\rangle_{\bar{1}}, \tag{7}$$

where $|\phi_i^{3;\kappa}\rangle_1$ refers to the first boson of the κ species in the state of $|\phi_i^{3;\kappa}\rangle$ and $|\vec{n}_\kappa - \hat{i}\rangle_{\bar{1}}$ is the permanent state of the remaining $N_\kappa - 1$ bosons of the κ species, with $|\vec{n}_\kappa - \hat{i}\rangle_{\bar{1}} = |(n_1, \ldots, n_i - 1, \ldots, n_{m_\kappa})\rangle_{\bar{1}}$. This is equivalent to dividing the Hilbert space of the κ species as $\mathscr{H}^\kappa = \mathscr{H}^{\kappa;1} \otimes \mathscr{H}^{\kappa;\bar{1}}$, where $\mathscr{H}^{\kappa;1}$ is the Hilbert space of the first κ boson spanned by the vectors of $\{|\phi_i^{3;\kappa}\rangle_1\}|_{i=1}^{m_\kappa}$ and $\mathscr{H}^{\kappa;\bar{1}}$ is the Hilbert space of the remaining $N_\kappa - 1$ bosons, spanned by the vectors of $\{|\vec{n}_\kappa\rangle_{\bar{1}} \equiv |(n_1, \ldots, n_{m_\kappa})\rangle_{\bar{1}} | \sum_{i=1}^m n_i = N_\kappa - 1\}$. Similarly, we can define the permanent state $|\vec{n}_\kappa\rangle_{\bar{l}}$, which includes all the κ bosons except the lth κ boson.

Now $|\delta\Psi\rangle$ and $\partial_t|\Psi\rangle$ can be written as

$$|\delta\Psi\rangle = \sum_I \delta A_I^1 |I\rangle + \sum_{\kappa,i,\vec{n}_\kappa} \delta A_{i;\vec{n}_\kappa}^{2;\kappa} |\vec{n}_\kappa\rangle \left|\tilde{\Psi}_i^{2;\kappa}\right\rangle + \sum_{\kappa,l,i,s} \delta A_{i;s}^{3;\kappa} \left|r_s^\kappa\right\rangle_l \left|\tilde{\Psi}_i^{3;\kappa}\right\rangle_{\bar{l}}; \tag{8}$$

$$\partial_t|\Psi\rangle = \sum_I (\partial_t A_I^1)|I\rangle + \sum_{\kappa,i,\vec{n}_\kappa} \left(\partial_t A_{i;\vec{n}_\kappa}^{2;\kappa}\right)|\vec{n}_\kappa\rangle \left|\tilde{\Psi}_i^{2;\kappa}\right\rangle + \sum_{\kappa,l,i,s} \left(\partial_t A_{i;s}^{3;\kappa}\right) \left|r_s^\kappa\right\rangle_l \left|\tilde{\Psi}_i^{3;\kappa}\right\rangle_{\bar{l}}. \tag{9}$$

In Eq. (8), the first term refers to the expansion of $|\delta\Psi\rangle$ with respect to the top-node coefficients with $|I\rangle \equiv \prod_{\kappa=1}^s |\phi_{i_\kappa}^{2;\kappa}\rangle$ and $I \equiv (i_1, \ldots, i_S)$, while the last two terms refer to the expansion over the species and particle SPFs. We introduce the single-hole function (SHF) $|\tilde{\Psi}_i^{\alpha;\kappa}\rangle$ for each SPF as $|\Psi\rangle =: \sum_i |\phi_i^{\alpha;\kappa}\rangle|\tilde{\Psi}_i^{\alpha;\kappa}\rangle$ with i summing over all the SPFs of the related node, and the SHFs of the species and particle layer are given as

$$\left|\tilde{\Psi}_j^{2;\kappa}\right\rangle = \sum_{I^\kappa} A_{I_j^\kappa}^1 \prod_{\mu\neq\kappa} \left|\phi_{i_\mu}^{2;\mu}\right\rangle, \tag{10}$$

$$\left|\tilde{\Psi}_j^{3;\kappa}\right\rangle_{\bar{l}} = \sum_i \sum_{\vec{n}_\kappa | N_\kappa - 1} \sqrt{\frac{n_j + 1}{N_\kappa}} A_{i;\vec{n}_\kappa + \hat{j}}^{2;\kappa} |\vec{n}_\kappa\rangle_{\bar{l}} \left|\tilde{\Psi}_i^{2;\kappa}\right\rangle. \tag{11}$$

In Eq. (10), I^κ is defined as an integer array of $(i_1, i_2, \ldots, i_{\kappa-1}, i_{\kappa+1}, \ldots, i_s)$, i.e., taking the index of i_κ out of I, and I_j^κ is defined as $(i_1, i_2, \ldots, i_{\kappa-1}, j, i_{\kappa+1}, \ldots, i_s)$. Comparing Eqs. (8) and (9), the time derivative of $|\Psi\rangle$ has the same overall structure as $|\delta\Psi\rangle$.

The equations of motion are derived by substituting Eqs. (8) and (9) into the Dirac-Frenkel variational principle and applying the restriction of $\langle\phi_i^{\alpha;\kappa}|\partial_t|\phi_j^{\alpha;\kappa}\rangle = 0$, for ensuring the orthonormality of the SPFs. In Eqs. (8) and (9), we

may only focus exclusively on $l = 1$ in the summation over l in the last term, as for each species κ the terms of different l are identical to each other due to the indistinguishability of the bosons belonging to the same species. Due to the same reason, we drop the subscripts of l and $\bar{l}$ for the permanents and SHFs in the following. The equations of motion for the coefficients read as

$$i\,\partial_t A^1_I = \sum_J \langle I|H|J\rangle A^1_J, \tag{12}$$

$$i\,\partial_t A^{\alpha;\kappa}_{n;C} = \sum_{m,D}\sum_p \langle C^{\alpha;\kappa}|(1-\hat{P}^{\alpha;\kappa})(\rho^{\alpha;\kappa})^{-1}_{n,p}\langle\hat{H}\rangle^{\alpha;\kappa}_{p,m}|D^{\alpha;\kappa}\rangle A^{\alpha;\kappa}_{m;D}. \tag{13}$$

In Eq. (13), $|C^{\alpha;\kappa}\rangle$ and $|D^{\alpha;\kappa}\rangle$ belong to the basic basis of the corresponding node, i.e., the basis used to build up the SPFs of the related node. For the species nodes, the basic basis is the permanent state basis $\{|\vec{n}_\kappa\rangle|N_\kappa\}$, and that of a particle node is $\{|r^\kappa_j\rangle\}_{j=1}^{\mathscr{M}_\kappa}$. The projection operator $\hat{P}^{\alpha;\kappa}$ is then defined as $\hat{P}^{\alpha;\kappa} = \sum_{i,E,F}(A^{\alpha;\kappa}_{i;F})^* A^{\alpha;\kappa}_{i;E}|E^{\alpha;\kappa}\rangle\langle F^{\alpha;\kappa}|$.

We also introduce in Eq. (13) the concepts of density matrices and mean-field operators, as follows:

$$(\rho^{\alpha;\kappa})_{i,j} = \left\langle\tilde{\Psi}^{\alpha;\kappa}_i\middle|\tilde{\Psi}^{\alpha;\kappa}_j\right\rangle, \tag{14}$$

$$\langle\hat{H}\rangle^{2;\kappa}_{i,j} = \sum_{\vec{n}_\kappa,\vec{m}_\kappa}\left\langle\tilde{\Psi}^{2;\kappa}_i\middle|\langle\vec{n}_\kappa|\hat{H}|\vec{m}_\kappa\rangle\middle|\tilde{\Psi}^{2;\kappa}_j\right\rangle|\vec{n}_\kappa\rangle\langle\vec{m}_\kappa|, \tag{15}$$

$$\langle\hat{H}\rangle^{3;\kappa}_{i,j} = \sum_{r^\kappa_1,r^\kappa_2}\left\langle\tilde{\Psi}^{3;\kappa}_i\middle|\left\langle r^\kappa_1\middle|\hat{H}\middle|r^\kappa_2\right\rangle\middle|\tilde{\Psi}^{3;\kappa}_j\right\rangle|r^\kappa_1\rangle\langle r^\kappa_2|. \tag{16}$$

Please note that $(\rho^{\alpha;\kappa})^{-1}_{n,p}$ in Eq. (13) refers to the (n,p)th element of the inverse of the regularized[2] density matrix (14). The above equations demonstrate the equations of motion for the coefficients in all layers of species ML-MCTDHB, and with these equations the time evolution of the system can be deduced.

Equations (12) and (13) give the general form of the equations of motion for species ML-MCTDHB, as well as the particle ML-MCTDHB, which will be introduced in Sec. II B. It turns out that the equations of motion for ML-MCTDHB take the same form of ML-MCTDH, despite that the two methods are dealing with indistinguishable and distinguishable particles, respectively. The difference between the two methods comes in the calculation of the ingredients of the equations, i.e., the density matrices and mean-field operators introduced in Eqs. (14)–(16). The formal similarity of the equations of motion of ML-MCTDHB and ML-MCTDH offers the possibility to merge the two methods together, and deal with mixtures consisting of distinguishable and indistinguishable particles.

3. Details and construction of the ingredients for the equations of motion

In Sec. II A 2, we have introduced the general form of the equations of motion with all necessary ingredients in Eqs. (12)–(16). In this section, we present the detailed expressions for the equations on different layers, with a focus on the second-quantization treatment on the bosonic species layer and particle layer. As this section mainly supplies the explicated equations of motion, it will not affect the understanding of the whole method to skip the detailed expressions in this section. Here, we consider a general Hamiltonian (1) containing single-particle terms, as well as two-body interaction terms. We adapt the product form representation of the interaction potentials, rewriting the intra- and inter-species interactions as

$$V_\kappa(r^\kappa_1, r^\kappa_2) = \sum_{n=1}^{\mathscr{V}_\kappa} C^\kappa_n V^\kappa_{n,1}(r^\kappa_1)V^\kappa_{n,2}(r^\kappa_2),$$
$$W_{\kappa_1\kappa_2}(r^{\kappa_1}_1, r^{\kappa_2}_2) = \sum_{n=1}^{\mathscr{W}_{\kappa_1,\kappa_2}} D^{\kappa_1,\kappa_2}_n W^{\kappa_1\kappa_2}_{n,\kappa_1}(r^{\kappa_1}_1)W^{\kappa_1\kappa_2}_{n,\kappa_2}(r^{\kappa_2}_2). \tag{17}$$

In (17), $V^\kappa_{n,p}$ and $W^{\kappa_1\kappa_2}_{n,\kappa_p}$ $(p = 1, 2)$ form the expansion basis of the product representations of the intra- and inter-species interactions $V_\kappa(r^\kappa_1, r^\kappa_2)$ and $W_{\kappa_1\kappa_2}(r^{\kappa_1}_1, r^{\kappa_2}_2)$, respectively. C^κ_n and D^{κ_1,κ_2}_n are the expansion coefficients for the intra- and inter-species interactions. Please note that one can bring any interaction potential to the product form (17). A convenient way of choosing the basis for the one-body operators $V^\kappa_{n,p}$ and $W^{\kappa_1\kappa_2}_{n,\kappa_p}$ $(p = 1, 2)$ is given by the algorithm POTFIT,[36,37] by using the basis of the so-called natural potentials. The natural potentials, for instance, $V^\kappa_{n,1}$ are defined as the eigenvectors of the potential density matrix $(V^\kappa)_{ij} = \sum_{r^\kappa=1}^{\mathscr{M}_\kappa} V_\kappa(r^\kappa_i, r^\kappa)^* V_\kappa(r^\kappa_j, r^\kappa)$. Consequently, C^κ_n is the overlap between V_κ and the product $V^\kappa_{n,1}V^\kappa_{n,2}$. The product form of the interactions allows the equations of motion to be expressed in a neat manner, and can improve the numerical performance if only a few terms are sufficient for a fair representation of the interaction potentials.

In ML-MCTDHB, the SPFs basis of each layer are truncated with respect to the lower layer, and the operators composing the Hamiltonian (1) can be expanded in the SPFs basis of each layer. Now we demonstrate the operator expansion with respect to the SPFs basis of each layer, and for the particle layer it is convenient to use the second quantization representation for the operators. The single particle operators, with respect to the equation of motion (13) for $\alpha = 3$, including the single particle Hamiltonian terms and $\hat{W}^{3;\kappa_1,\kappa_2}_{n,\kappa_p}$ $(p = 1, 2)$ for inter-species interaction terms, are given on the particle layer as follows:

$$\hat{H}^{3;\kappa}_0 = \sum_{i,j}\left(H^{3;\kappa}_0\right)_{ij}\hat{a}^\dagger_{\kappa,i}\hat{a}_{\kappa,j},$$
$$\hat{W}^{3;\kappa_1,\kappa_2}_{n,\kappa_p} = \sum_{i,j}\left(W^{3;\kappa_1,\kappa_2}_{n,\kappa_p}\right)_{ij}\hat{a}^\dagger_{\kappa_p,i}\hat{a}_{\kappa_p,j} \qquad (p = 1, 2). \tag{18}$$

Here, $\hat{a}_{\kappa,i}$ $(\hat{a}^\dagger_{\kappa,i})$ refers to the operator annihilating (creating) a κ boson in the SPF state $|\phi^{3;\kappa}_i\rangle$. $(H^{3;\kappa}_0)_{ij}$ is defined as $(H^{3;\kappa}_0)_{ij} \equiv \langle\phi^{3;\kappa}_i|\hat{H}^0_\kappa|\phi^{3;\kappa}_j\rangle$, and $(W^{3;\kappa_1,\kappa_2}_{n,\kappa_p})_{ij}$ follows the same definition. The two-particle operators for the intra-species

interactions are given as

$$\hat{V}^{3;\kappa} = \frac{1}{2}\sum_{i_1,i_2,j_1,j_2}(V^{3;\kappa})_{i_1 i_2 j_1 j_2}\hat{a}^{\dagger}_{\kappa,i_1}\hat{a}^{\dagger}_{\kappa,i_2}\hat{a}_{\kappa,j_1}\hat{a}_{\kappa,j_2} = \frac{1}{2}\sum_{n} C^{\kappa}_{n}\sum_{i_1,i_2,j_1,j_2}\left(V^{3;\kappa}_{n,1}\right)_{i_1 j_1}\left(V^{3;\kappa}_{n,2}\right)_{i_2 j_2}\hat{a}^{\dagger}_{\kappa,i_1}\hat{a}^{\dagger}_{\kappa,i_2}\hat{a}_{\kappa,j_1}\hat{a}_{\kappa,j_2}, \tag{19}$$

with $(V^{3;\kappa}_{n,p})_{ij} = \langle\phi^{3;\kappa}_i|\hat{V}^{\kappa}_{n,p}|\phi^{3;\kappa}_j\rangle$ $(p = 1, 2)$.

On the species layer, the terms of the single particle Hamiltonian become

$$\hat{H}^{2;\kappa}_0 = \sum_{ij}\left(H^{2;\kappa}_0\right)_{ij}\left|\phi^{2;\kappa}_i\right\rangle\left\langle\phi^{2;\kappa}_j\right|, \qquad \left(H^{2;\kappa}_0\right)_{ij} \equiv \sum_{p,q}\left(H^{3;\kappa}_0\right)_{pq}\left(\tilde{Q}^{\kappa}_{pq}\right)_{ij}. \tag{20}$$

The intra-species interaction operators also become effectively single particle operators with respect to the species SPFs, as

$$\hat{V}^{2;\kappa} = \sum_{ij}(V^{2;\kappa})_{ij}\left|\phi^{2;\kappa}_i\right\rangle\left\langle\phi^{2;\kappa}_j\right|, \qquad (V^{2;\kappa})_{ij} \equiv \frac{1}{2}\sum_{p_1 p_2 q_1 q_2}(V^{3;\kappa})_{p_1 p_2 q_1 q_2}\left(\tilde{P}^{\kappa}_{p_1 p_2 q_1 q_2}\right)_{ij}. \tag{21}$$

In Eqs. (20) and (21), we define

$$\left(\tilde{Q}^{\kappa}_{pq}\right)_{ij} = \sum_{\vec{n}|N_\kappa-1}\left(A^{2;\kappa}_{i;\vec{n}+\hat{p}}\right)^{*}A^{2;\kappa}_{j;\vec{n}+\hat{q}}\,Q_{\vec{n}}(p,q)$$

and

$$\left(\tilde{P}^{\kappa}_{p_1 p_2 q_1 q_2}\right)_{ij} = \sum_{\vec{n}|N_\kappa-2}\left(A^{2;\kappa}_{i;\vec{n}+\hat{p}_1+\hat{p}_2}\right)^{*}A^{2;\kappa}_{j;\vec{n}+\hat{q}_1+\hat{q}_2}\,P_{\vec{n}}(p_1,p_2)\times P_{\vec{n}}(q_1,q_2).$$

The summation index $\vec{n}|N_\kappa - k$ refers to all the permanent states of $(N-k)$ bosons, while $\vec{n}+\hat{q}$ and $\vec{n}+\hat{q}_1+\hat{q}_2$ refer to adding one boson to the qth SPF state of $\vec{n}$ and adding two bosons to the q_1th and q_2th SPF states of $\vec{n}$, respectively. We also introduce here $P_{\vec{n}}(l,m) = \sqrt{(n_l+1+\delta_{l,m})(n_m+1)}$ and $Q_{\vec{n}}(i,j) = \sqrt{(n_i+1)(n_j+1)}$. The single particle operators $\hat{W}^{2;\kappa_1,\kappa_2}_{n,p}$, are defined in the same way as the single particle Hamiltonian terms in Eq. (20).

Then we can show the detailed form of the equations of motion for the coefficients on all layers. The top layer equations of motion turn out to be

$$i\,\partial_t A^1_I = \sum_{\kappa}\sum_{j}\left[\left(H^{2;\kappa}_0\right)_{i_\kappa j} + (V^{2;\kappa})_{i_\kappa j}\right]A^1_{I^{\kappa}_j} + \sum_{\kappa_1<\kappa_2}\sum_{n}\sum_{j_1,j_2}D^{\kappa_1,\kappa_2}_{n}\left(W^{2;\kappa_1,\kappa_2}_{n,\kappa_1}\right)_{i_{\kappa_1} j_1}\left(W^{2;\kappa_1,\kappa_2}_{n,\kappa_2}\right)_{i_{\kappa_2} j_2}A^1_{I^{\kappa_1\kappa_2}_{j_1 j_2}}. \tag{22}$$

I is again defined as an array of $(i_1, i_2, \ldots, i_S)$, while I^{κ}_j and $I^{\kappa_1\kappa_2}_{j_1 j_2}$ are the arrays obtained by replacing i_κ in I by j and i_{κ_1}, i_{κ_2} in I by j_1, j_2, respectively.

The equations of motion for the coefficients on the non-top layers can be obtained by substituting the related density matrices and mean-field operators to Eq. (13). The density matrices on the species and particle layers are calculated, respectively, as

$$(\rho^{2;\kappa})_{ij} = \sum_{I^{\kappa}}\left(A^1_{I^{\kappa}_i}\right)^{*}A^1_{I^{\kappa}_j}, \qquad (\rho^{3;\kappa})_{ij} = \frac{1}{N_\kappa}\sum_{kl}\rho^{2;\kappa}_{kl}\left(\tilde{Q}^{\kappa}_{ij}\right)_{kl}. \tag{23}$$

On the species layer, the mean-field operators for the terms of the single particle Hamiltonian and intra-species interactions are calculated, in the second quantization picture, as

$$\left\langle\hat{H}^0_\kappa + \hat{V}_\kappa\right\rangle^{2;\kappa}_{ij} = (\rho^{2;\kappa})_{ij}\left(\hat{H}^{3;\kappa}_0 + \hat{V}^{3;\kappa}\right). \tag{24}$$

The mean-field operator for all inter-species interactions acting on the κ species is given by $\langle\hat{W}_\kappa\rangle^{2;\kappa}_{ij} = \sum_{\nu\neq\kappa}\langle\hat{W}_\kappa\rangle^{2;\kappa,\nu}_{ij}$, where the mean field operator for the inter-species interaction between the κ and ν species is obtained by $\langle\hat{W}_\kappa\rangle^{2;\kappa,\nu}_{ij} = \sum_{n=1}^{\mathscr{W}_{\kappa,\nu}} D^{\kappa,\nu}_n\langle\hat{W}_{n,\kappa}\rangle^{2;\kappa,\nu}_{ij}$ with

$$\langle\hat{W}_{n,\kappa}\rangle^{2;\kappa,\nu}_{ij} = \hat{W}^{3;\kappa,\nu}_{n,\kappa}\cdot\left(\tilde{W}^{2;\kappa,\nu}_{n,\kappa}\right)_{ij}, \qquad \left(\tilde{W}^{2;\kappa,\nu}_{n,\kappa}\right)_{ij} = \sum_{I^{\kappa,\nu}}\sum_{rs}\left(A^1_{I^{\kappa,\nu}_{i,r}}\right)^{*}A^1_{I^{\kappa,\nu}_{j,s}}\left(W^{2;\kappa,\nu}_{n,\nu}\right)_{rs}. \tag{25}$$

On the particle layer, the mean-field operators for the terms of the single particle Hamiltonian, the intra-species interactions, and the inter-species interactions are calculated by

$$\left\langle\hat{H}^0_\kappa\right\rangle^{3;\kappa}_{ij} = (\rho^{3;\kappa})_{ij}\hat{H}^0_\kappa, \qquad \langle\hat{V}_\kappa\rangle^{3;\kappa}_{ij} = \frac{1}{N_\kappa}\sum_{n=1}^{\mathscr{V}_\kappa}C^{\kappa}_n\langle\hat{V}_{n;\kappa}\rangle^{3;\kappa}_{ij}, \qquad \langle\hat{W}_\kappa\rangle^{3;\kappa}_{ij} = \frac{1}{N_\kappa}\sum_{\nu\neq\kappa}\sum_{n=1}^{\mathscr{W}_{\kappa,\nu}}D^{\kappa,\nu}_n\langle\hat{W}_{n,\kappa}\rangle^{3;\kappa,\nu}_{ij}, \tag{26}$$

with the mean field operators

$$\langle\hat{V}_{n;\kappa}\rangle^{3;\kappa}_{ij} \equiv \left(\hat{V}^{\kappa}_{n,1}\right)\left(\sum_{rs}(\rho^{2;\kappa})_{rs}\sum_{pq}\left(\tilde{P}^{\kappa}_{ipjq}\right)_{rs}\left(V^{3;\kappa}_{n,2}\right)_{pq}\right),$$

and

$$\langle\hat{W}_{n,\kappa}\rangle^{3;\kappa,\nu}_{ij} = \left(\hat{W}^{\kappa,\nu}_{n,\kappa}\right)\left(\sum_{rs}\left(\tilde{W}^{2;\kappa,\nu}_{n,\kappa}\right)_{rs}\left(\tilde{Q}^{\kappa}_{ij}\right)_{rs}\right).$$

Please note the recursive character of the formulas for the mean-field operators and the reduced density matrices, which is a consequence of the product representation of the interaction potentials. The equations of motion without the product representation of the interactions are given in the Appendix.

B. ML-MCTDHB for high-dimensional bosonic systems

Now we proceed to demonstrate the multi-layer treatment of high-dimensional bosonic systems, which is termed as particle ML-MCTDHB. Particle ML-MCTDHB has its origin in the mode combination of MCTDH,[4] as well as the multi-layer scheme of ML-MCTDH.[8] In this section, we take a

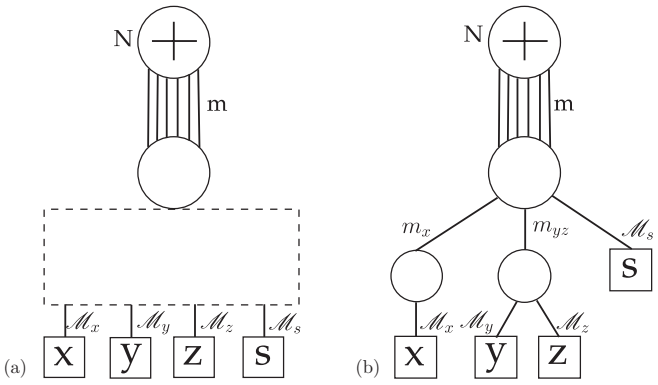

FIG. 2. (a) An illustration of a general particle multi-layer MCTDHB wave function expansion for spin-one bosons in three-dimensional coordinate space, with $\mathscr{M}_s = 3$ in the figures. The dashed box indicates the various possibilities for mode combination of the primitive DOF, i.e., the spatial DOF x, y, z and the spin projection on the z-axis. (b) An example of the mode combination scheme inside the dashed box of (a), where the spatial DOF y and z are combined into one logical DOF.

single-species bosonic system in high-dimensional space as an example to demonstrate the particle ML-MCTDHB, and the combination of species and particle ML-MCTDHB will be given in Sec. II C. This example also shows how ML-MCTDHB deals with a single-species system, which is also a supplement to the general discussion of bosonic mixtures in Secs. II A 1–II A 3. We consider a single-species bosonic system of N identical bosons living in a Q-dimensional configuration space, spanned by the primitive DOF $\{x_1, x_2, \ldots, x_Q\}$. In ML-MCTDHB, we first perform a mode combination of these primitive DOF, and generate the logical DOF one layer above, as

$$\begin{aligned} x_1^{P-1} &= x_1^{P-1}(x_1, x_2, \ldots, x_{n_1}), \\ x_2^{P-1} &= x_2^{P-1}(x_{n_1+1}, x_{n_1+2}, \ldots, x_{n_1+n_2}), \\ &\vdots \\ x_{N_{P-1}}^{P-1} &= x_{N_{P-1}}^{P-1}(x_{N-n_{N_P}+1}, x_{N-n_{N_P}+2}, \ldots, x_Q). \end{aligned} \tag{27}$$

Such mode combination can be repeated recursively layer by layer, until all the DOF are combined into a single logical DOF, which correspond to the particle node. Above this particle node, there is the top node representing the state vector $|\Psi\rangle$ of the whole system. This mode-combination procedure corresponds to the tree structure shown in Figure 2(a), where the bottom nodes are the so-called primitive nodes, containing the primitive DOF, and the dashed box between the particle node and the primitive nodes indicates the variety of possible mode-combination schemes.

For each primitive DOF, a set of time-independent basis vectors is assigned. Above the primitive nodes, a set of time-dependent SPFs is associated to each logical DOF on the non-top layer, which are expanded with respect to the SPFs of the corresponding DOF one layer below, as

$$\left|\phi_n^{\alpha;\kappa}\right\rangle = \sum_{i_1,i_2,\ldots,i_m} A_{n;i_1,i_2,\ldots,i_m}^{\alpha;\kappa} \prod_{r\in M^{\alpha;\kappa}} \left|\phi_{i_r}^{\alpha+1;\kappa_r}\right\rangle \equiv \sum_I A_{n;I}^{\alpha;\kappa} |I^{\alpha;\kappa}\rangle. \tag{28}$$

Here, $|\phi_n^{\alpha;\kappa}\rangle$ is the nth SPF of the κth DOF on the αth layer, and this logical DOF is a combination of a set $M^{\alpha;\kappa}$ of m DOF of the lower layer, where $M^{\alpha;\kappa}$ keeps track of the correct subnode indices κ_r belonging to the node $(\alpha;\kappa)$. The state vector $|\Psi\rangle$ of the top node is expanded with respect to permanents

$$|\Psi\rangle = \sum_{\vec{n}|N} A_{\vec{n}}^1 |\vec{n}\rangle. \tag{29}$$

An example for incorporating primitive mode combination in particle ML-MCTDHB is shown in Figure 2(b). The tree structure in Figure 2(b) corresponds to a single-species bosonic ensemble, and the bosons possess four primitive DOF, i.e., the three spatial DOF along x, y, and z directions as well as an internal DOF, e.g., a spin DOF. In the mode combination shown here, the y and z DOF are grouped into one logical DOF, and the primitive basis of x DOF is truncated to a set of SPF, associated with a logical DOF. Then these two logical DOF are combined with the internal primitive DOF to the upper layer logical DOF represented by the particle node. Physically, this mode combination might correspond, as an example, to the strongly correlated y and z DOF with weak correlation to x DOF.

For simplicity, we restrict ourselves to two-body interactions and, moreover, assume the product form representations of the Hamiltonian as usual

$$\begin{aligned} \hat{H} &= \sum_i \hat{h}(i) + \sum_{i<j} \hat{V}(i,j) \\ &= \sum_i \hat{h}(i) + \sum_{i<j} \sum_\nu C_\nu \hat{v}_\nu^1(i) \hat{v}_\nu^2(j). \end{aligned} \tag{30}$$

$\hat{h}(i)$ and $\hat{V}(i,j)$ are the one-body Hamiltonian acting on the ith boson, and the two-particle interaction operator acting on the ith and jth bosons, respectively, where the two-particle interaction operator is written as the summation of products of single particle operators acting on the ith and jth boson separately.

The equations of motion of all the coefficients are again obtained by the Dirac-Frenkel variational principle and the equations for the top and particle nodes read

$$\begin{aligned} i\,\partial_t A_{\vec{n}}^1 &= \sum_{\vec{m}} \langle \vec{n}|\hat{H}|\vec{m}\rangle A_{\vec{m}}^1, \\ i\,\partial_t A_{n;I}^{2;1} &= \sum_J \langle I^{2;1}|(1-\hat{P}^{2;1})\hat{h}|J^{2;1}\rangle A_{n;J}^{2;1} \\ &\quad + \sum_\nu C_\nu \left\{ \sum_J \langle I^{2;1}|(1-\hat{P}^{2;1})\hat{v}_{\nu;1}|J^{2;1}\rangle \right\} \\ &\quad \times \left\{ \sum_m \left[(\rho^{2;1})^{-1} \times \langle \tilde{v}_{\nu;2}^{2;1}\rangle\right]_{n,m} \right\} A_{m;J}^{2;1}. \end{aligned} \tag{31}$$

For the particle node, $\hat{P}^{2;1} \equiv \sum_n |\phi_n^{2;1}\rangle\langle\phi_n^{2;1}|$ is the projection operator, and for the single species case there is only one node on the particle layer, we have $\kappa = 1$ on this layer. The density matrix $\rho^{2;1}$ is calculated as

$$\rho_{ij}^{2;1} = \frac{1}{N} \sum_{\vec{n}|N-1} Q_{\vec{n}}(i,j) \left(A_{\vec{n}+\hat{i}}^1\right)^* A_{\vec{n}+\hat{j}}^1, \tag{32}$$

and the mean-field matrices $\langle \tilde{v}^{2;1}_{\nu;2} \rangle$ are calculated as

$$\langle \tilde{v}^{2;1}_{\nu;2} \rangle_{i,j} = \frac{1}{N} \sum_{\vec{n}|N-2} \sum_{p,q} P_{\vec{n}}(i,p) P_{\vec{n}}(j,q) \left(A^1_{\vec{n}+\hat{i}+\hat{p}}\right)^* A^1_{\vec{n}+\hat{j}+\hat{q}} \times \langle \phi^{2;1}_p | \hat{v}^2_\nu | \phi^{2;1}_q \rangle. \quad (33)$$

Assuming that the one-body operators $\hat{h}$, $\hat{v}^i_\nu$ (i = 1,2) are also given in a product form with respect to the primitive DOF, these operators can be expressed with respect to the logical DOF of each layer on the layers below the particle layer (cf. Ref. 8), e.g.,

$$\hat{h}^{\alpha;\kappa} = \sum_\mu D_\mu \prod_\kappa \hat{h}^{\alpha;\kappa}_\mu. \quad (34)$$

Here, $\hat{h}^{\alpha;\kappa}_\mu$ is an operator acting on the $(\alpha;\kappa)$ DOF, and can be obtained recursively by $(\hat{h}^{\alpha;\kappa}_\mu)_{ij} = \langle \phi^{\alpha;\kappa}_i | \prod_{\nu \in M^{\alpha;\kappa}} \hat{h}^{\alpha+1;\nu}_\mu | \phi^{\alpha;\kappa}_j \rangle$. Then the density and mean-field matrices of the logical DOF below the particle layer are generated the same way as in ML-MCTDH, which enables one to apply the well-known recursion schemes.[8,9] The equations of motion can then be obtained by substituting the related operators, density matrices, and mean-field matrices to Eq. (13), which turns out to be general for both the species and particle ML-MCTDHB.

C. ML-MCTDHB for general bosonic systems

In this section, we demonstrate the general ML-MCTDHB theory which is a combination of the species ML-MCTDHB and particle ML-MCTDHB. The general ML-MCTDHB approach extends our study to bosonic mixtures in high-dimensional systems and even mixed-dimensional systems. As an example, we consider a three-species bosonic mixture in three-dimensional space, and the three species are again named as A, B, and C bosons. First, a tree diagram related to this three-species mixture is given in Figure 3. This three-species mixture is different from the mixture in Figure 1 by the fact that the A and B bosons have three primitive DOF in Figure 3. Despite the difference, the tree diagrams for both mixtures have the same structure from top to particle layer, which indicates that the setup on the particle multi-layer level will not affect the species multi-layer level, which is above the particle layer. On the particle multi-layer level, the three species follow different mode combination schemes, determined by the correlations between the DOF of each boson. The different mode combinations of the three species in Figure 3 indicate that the three DOF of A bosons are all strongly correlated, while for B bosons only the x and y DOF are strongly correlated, which are combined together, and the three DOF of C bosons have loose correlations between each other. The *Ansatz* for A, B, and C bosons on the particle multi-layer level can be obtained following the discussion in Sec. II B. To conclude, the species and particle ML-MCTDHB are actually independent of each other, and they can be straightforwardly connected on the particle layer. The structure of the species level only depends on the correlations between the bosonic species, while the structure on the particle level is determined by the correlations of the primitive DOF.

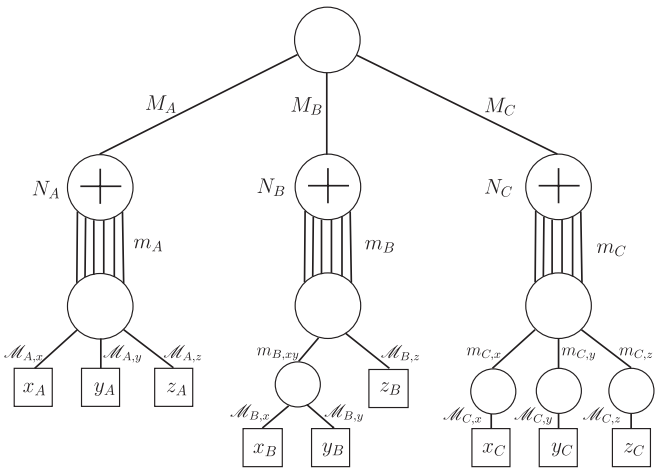

FIG. 3. A tree diagram of the combined treatment of the species and particle ML-MCTDHB for a three-species bosonic system. The three species are again labeled as A, B, and C bosons as in Figure 1. In contrast to that example, the bosons of all species may move in three-dimensional space here.

Similar to the *Ansatz* for the combination of species and particle ML-MCTDHB, the equations of motion are compatible with each other. A brief sketch of the link between species and particle ML-MCTDHB goes as follows: At each time step, the Hamiltonian operators are generated for each layer from primitive to top layer, then the density matrices and mean-field operators are constructed from top to bottom. The calculation of the Hamiltonian operators, density matrices, and the mean-field operators on a certain layer follows the corresponding rules given in Secs. II A and II B. Substituting all the components into the corresponding equations, the right hand side (rhs) of the equations of motion is ready to be handed to the integrator.

For the calculation of the equations, one point not mentioned in Sec. II B are the mean-field operators of the interspecies interactions on the particle multi-layer level. For this point, we consider a general case of interspecies interaction between the κ_1 and κ_2 bosons. On the αth layer below the particle layer, this interaction is written in the POTFIT form as $\hat{W}^{\alpha;\kappa_1,\kappa_2} = \sum_n D^{\alpha;\kappa_1,\kappa_2}_n (\prod_{i=1}^{m^{\alpha,\kappa_1}} \hat{W}^{\alpha;\kappa_1,\kappa_2}_{n,\kappa_1,i}) (\prod_{j=1}^{m^{\alpha,\kappa_2}} \hat{W}^{\alpha;\kappa_1,\kappa_2}_{n,\kappa_2,j})$, where there are m^{α,κ_1} and m^{α,κ_2} DOF for the κ_1 and κ_2 bosons on the α layer. Assuming that the mean-field operator for the interspecies interaction on the particle layer has been calculated by Eq. (33), the mean-field operator on the α-layer below the particle layer can be calculated as

$$\begin{aligned} \langle \hat{W}^{\alpha;\kappa_1,\kappa_2}_{n,\kappa_1,a} \rangle_{ij} &= \left(\hat{W}^{\alpha+1;\kappa_1,\kappa_2}_{n,\kappa_1,a}\right) \langle \tilde{W}^{\alpha;\kappa_1,\kappa_2}_{n,\kappa_1,a} \rangle_{ij}, \\ \langle \tilde{W}^{\alpha;\kappa_1,\kappa_2}_{n,\kappa_1,a} \rangle_{ij} &= \sum_{rs} \langle \tilde{W}^{\alpha-1;\kappa_1,\kappa_2}_{n,\kappa_1,b} \rangle_{rs} \sum_{I^a} \sum_{J^a} \left(A^{\alpha-1;\kappa_1}_{r;I^a_i}\right)^* A^{\alpha-1;\kappa_1}_{s;J^a_j} \\ &\quad \times \prod_{\substack{p \in M^{\alpha-1;\kappa_1,b} \\ p \neq a}} \left(W^{\alpha,\kappa_1,\kappa_2}_{n,\kappa_1,p}\right)_{i_p,j_p}, \end{aligned} \quad (35)$$

where $M^{\alpha-1;\kappa_1,b}$ is the set of α-layer DOF combined into the bth DOF of the κ_1 species and $(W^{\alpha,\kappa_1,\kappa_2}_{n,\kappa_1,p})_{i_p,j_p}$ are the matrix elements of the corresponding operator. For a more detailed description of the mean-field operators, we refer to Ref. 8.

TABLE I. The scaling of the methods MCTDH, ML-MCTDH, MCTDH-BB, and ML-MCTDHB is compared for the case of $S = 2$ species, $m = 4$ particle SPFs, and $n = 250$ spatial grid points. The number of bosons per species, N, and (for the multi-layer methods) the number of species SPFs, M, are varied. Each table entry contains the number of coefficients needed for the wave function expansion of the respective method and its ratio with respect to the number of ML-MCTDHB coefficients.

(N, M)	MCTDH	ML-MCTDH	MCTDH-BB	ML-MCTDHB
(4,2)	$7.4 \times 10^4/34.3$	$9.0 \times 10^3/4.2$	$3.2 \times 10^3/1.5$	$2.1 \times 10^3/1.0$
(4,6)	$7.4 \times 10^4/30.0$	$1.1 \times 10^4/4.5$	$3.2 \times 10^3/1.3$	$2.5 \times 10^3/1.0$
(4,14)	$7.4 \times 10^4/23.2$	$1.5 \times 10^4/4.8$	$3.2 \times 10^3/1.02$	$3.2 \times 10^3/1.0$
(4,16)	$7.4 \times 10^4/21.8$	$1.6 \times 10^4/4.9$	$3.2 \times 10^3/0.96$	$3.4 \times 10^3/1.0$
(4,35)	$7.4 \times 10^4/13.0$	$2.7 \times 10^4/4.8$	$3.2 \times 10^3/0.6$	$5.7 \times 10^3/1.0$
(40,1)	$1.5 \times 10^{48}/5.5 \times 10^{43}$	$2.4 \times 10^{24}/9.1 \times 10^{19}$	$1.5 \times 10^8/5.7 \times 10^3$	$2.7 \times 10^4/1.0$
(40,2)	$1.5 \times 10^{48}/2.8 \times 10^{43}$	$4.8 \times 10^{24}/9.4 \times 10^{19}$	$1.5 \times 10^8/3.0 \times 10^3$	$5.1 \times 10^4/1.0$
(40,3)	$1.5 \times 10^{48}/1.9 \times 10^{43}$	$7.3 \times 10^{24}/9.5 \times 10^{19}$	$1.5 \times 10^8/2.0 \times 10^3$	$7.6 \times 10^4/1.0$
(40,4)	$1.5 \times 10^{48}/1.5 \times 10^{43}$	$9.7 \times 10^{24}/9.6 \times 10^{19}$	$1.5 \times 10^8/1.5 \times 10^3$	$1.0 \times 10^5/1.0$

The general ML-MCTDHB method can deal with bosonic mixtures in high-dimensional space and even mixed dimensions, and a major advantage of the method lies in its flexibility with respect to the SPFs of each DOF. The method can handle both the weak and strong correlation regimes, simply by adjusting the number of the SPFs of related DOF. For instance, when the intra- and inter-species interactions are weak, we can take few particle and species SPFs, and the extreme case is that we take only one particle and one species SPF for each species, which reduces to the mean-field treatment. On the other hand, in the case of strong intra-species interaction but weak inter-species interaction, we need to supply more particle SPFs, but few species SPFs. One can also reach the full CI limit by supplying as many SPFs for each DOF as the basic basis states of the corresponding DOF.

D. Scaling

At this stage, we would like to point out the relationship between ML-MCTDHB and related methods. For a single-species system, ML-MCTDHB and MCTDHB[10–12] coincide for one-dimensional bosons without internal degrees of freedom. When considering a single species of bosons living in a higher-dimensional configuration space, e.g., with both spatial and internal DOF, ML-MCTDHB reduces to MCTDHB if all the primitive modes are directly combined to the particle node. For bosonic mixtures, MCTDHB has been generalized to deal with mixtures, e.g., containing two or three bosonic species, with methods known as MCTDH-BB[20] and MCTDH-BBB,[21] respectively. In the following, we categorize them as standard MCTDHBs in comparison to the multi-layer MCTDHB. The state vector of the total system is expanded in standard MCTDHBs as the summation over the products of the permanents states belonging to each species, while in species multi-layer MCTDHB the state vector is first expanded with respect to Hartree products of species SPFs, and the species SPFs are then expanded within the permanents basis of each species. Hence, ML-MCTDHB recovers the standard MCTDHBs treatment if as many species SPFs are provided as there are configurations for each species.

We finally compare the scaling of the methods MCTDH, ML-MCTDH, standard MCTDHBs, and ML-MCTDHB applied to a multi-species setup by investigating the memory consumption for storing the total wave function. This also provides us with a rough estimate for the performances of the methods. Let us consider a bosonic mixture of S species, of which each species contains N bosons, and we denote the number of grid points and particle SPFs by n and m, respectively. If we neglect the symmetrization option as well as the possibility of primitive mode combination, $m^{SN} + SNmn$ coefficients have to be propagated in MCTDH. The ML-MCTDH expansion equivalent to the species ML-MCTDHB expansion, where one replaces the expansion (4) by an expansion in terms of Hartree products made of the SPFs $|\phi_i^{3;\kappa}\rangle$, requires $M^S + SMm^N + SNmn$ coefficients, where M is the number of species SPFs of each species. For a direct standard MCTDHBs expansion, one needs $\binom{N+m-1}{m-1}^S + Smn$ coefficients. Finally, the species ML-MCTDHB *Ansatz* consists of $M^S + SM\binom{N+m-1}{m-1} + Smn$ coefficients. Table I lists the memory consumption of the different methods for $S = 2$ species, $n = 250$ spatial grid points, $m = 4$ particle SPFs, and various numbers of bosons in each species, N, and species SPFs, M. If the necessary number of species SPFs is not too large with respect to the total number of bosonic configurations, $\binom{N+m-1}{m-1}$, ML-MCTDHB clearly requires less memory than all the other methods. In the case of the two species example and $N = 40$, $M = 4$, the ML-MCTDHB wave function *Ansatz* consists of three orders of magnitude less coefficients than the corresponding MCTDH-BB *Ansatz*. For large numbers of species SPFs, however, a MCTDH-BB expansion becomes preferable with respect to the memory consumption, which can be seen from the $N = 4$ and $M = 16, 35$ example in Table I.

Obviously, the number of species and particle SPFs, i.e., (M,m), needed for a converged simulation does strongly depend on the details of the system: The more correlations and entanglement are present in the system the more of these basis functions are required. In view of this, Table I serves as an exemplary overview over the (M,m) parameter space being accessible by ML-MCTDHB but not or hardly by other methods. For instance, we can interpret the last row of Table I as that ML-MCTDHB can simulate a particular parameter regime of a two-species bosonic mixture containing 40 bosons of each species, where the simulation is converged with the given (M,m), while the huge number of expansion

coefficients prevent other methods to reach any parameter regime except where a mean-field approximation is valid.

E. Symmetry conservation

Let us focus next on the symmetry conservation property of ML-MCTDHB. The discussion in this section can be extended to the complete MCTDH family, including MCTDH, ML-MCTDH, and MCTDHB(F). It is already known that the equations of motion of the MCTDH family preserve the total energy and the normalization of the wave function.[2] Here, we show that the equations also preserve a certain class of symmetries, given that the initial wave function and the SPFs on each level possess this symmetry. To illustrate this idea, we focus on the particle ML-MCTDHB and assume that the Hamiltonian $\hat{H}$ has some symmetry group $\mathcal{G}$ and let $\hat{G}$ be an element of the unitary representation of $\mathcal{G}$ in the many-body Hilbert space, i.e., $[\hat{G}, \hat{H}] = 0$. We hereby only consider symmetry operations which can be decomposed as $\hat{G} = \bigotimes_i \hat{g}_i$, where $\hat{g}_i$ is an element of the unitary representation of $\mathcal{G}$ in the Hilbert space of the ith primitive DOF. (Some of the $\hat{g}_i$th may be the unit operator.) $\hat{G}$ can be further represented as a product of operators acting on the κth logical DOF of the αth layer: $\hat{G} = \bigotimes_\kappa \hat{g}^{\alpha;\kappa}$. Let us assume that initially the total wave function and all SPFs are invariant under the respective symmetry operators, i.e., $\hat{G}|\Psi(0)\rangle = e^{i\Theta}|\Psi(0)\rangle$ and $\hat{g}^{\alpha;\kappa}|\phi_j^{\alpha;\kappa}(0)\rangle = e^{i\theta_j^{\alpha;\kappa}}|\phi_j^{\alpha;\kappa}(0)\rangle$. Then the Hamiltonian matrix $\langle\vec{n}|\hat{H}|\vec{m}\rangle$ in (31) does not allow transitions from the permanent state $|\vec{m}\rangle$ with $\hat{G}|\vec{m}\rangle = e^{i\Theta'}|\vec{m}\rangle$ to $|\vec{n}\rangle$ with $\hat{G}|\vec{n}\rangle = e^{i\Theta''}|\vec{n}\rangle$ and $\Theta' \mod 2\pi \neq \Theta'' \mod 2\pi$, when propagating the coefficients for a small time step Δt, i.e., $\langle\vec{n}|\hat{H}|\vec{m}\rangle$ vanishes for such permanent states. Hence, we are left to show that the SPFs preserve their symmetry up to $O(\Delta t^2)$ when propagating them for a small time step. We note that the mean-field operator matrices of a Hamiltonian containing at most F-body terms can be expressed by the F-body reduced density matrices and one-body operators. Now the initially well defined many-body symmetry, $A_{\vec{n}}(t=0) \neq 0 \Rightarrow \hat{G}|\vec{n}\rangle(t=0) = e^{i\Theta}|\vec{n}\rangle(t=0)$, implies that the F-body reduced density matrix elements $\rho^{F;\alpha;\kappa}_{i_1,\ldots,i_F;j_1,\ldots,j_F}$ can only be non-vanishing if $\sum_{r=1}^{F}\theta_{i_r}^{\alpha;\kappa} = \sum_{r=1}^{F}\theta_{j_r}^{\alpha;\kappa}$ up to integer multiples of 2π. This can be seen implicitly from the mean field matrices (33) in the example of two-body interactions. If we further group the initial SPFs $|\phi_j^{\alpha;\kappa}(0)\rangle$ into classes of the same $\theta_j^{\alpha;\kappa} \mod 2\pi$, the inverses of the one-body reduced density matrices in (32) are initially block diagonal. With these two observations, one can directly show $\hat{g}^{\alpha;\kappa}\partial_t|\phi_j^{\alpha;\kappa}(t)\rangle = e^{i\theta_j^{\alpha;\kappa}}\partial_t|\phi_j^{\alpha;\kappa}(t)\rangle$ at $t = 0$. The same arguments hold for any later time steps as long as Δt is small enough and the symmetry conservation becomes exact for $\Delta t \to 0$.

Following the proof, we conclude that if at $t = 0$ the many-body wave function $|\Psi(0)\rangle$ and all the SPFs $|\phi_j^{\alpha;\kappa}(0)\rangle$ are invariant under $\hat{G}$ and $\hat{g}^{\alpha;\kappa}$, respectively, they remain invariant for all times, i.e., $\hat{G}|\Psi(t)\rangle = e^{i\Theta}|\Psi(t)\rangle$ and $\hat{g}^{\alpha;\kappa}|\phi_j(t)\rangle = e^{i\theta_j^{\alpha;\kappa}}|\phi_j^{\alpha;\kappa}(t)\rangle$ for all t. Such an initial state preparation can be performed in ML-MCTDHB by choosing the initial SPFs as eigenstates of the single particle symmetry operators and populating only number states with the same many-body symmetry. Please note that this symmetry conservation property cannot be expected *a priori* due to the truncation of the many-body Hilbert space and the complicated integro-differential equations for the SPFs and to the best of our knowledge this has not been shown previously. Possibly this symmetry conservation can be employed for specifying the configuration selection in selected configuration MCTDH type methods (cf. Ref. 35 and references therein).

III. IMPLEMENTATION

A. Implementation of the second quantization formalism

In this section, we briefly comment on some technical details of the ML-MCTDHB algorithm, and we mainly focus on two issues: the permanent state sequencing and the second-quantization calculations, which manifest themselves as a major challenge in the numerical treatment of the bosonic systems.

A permanent state of $|\vec{n}\rangle = |(n_1, n_2, \ldots, n_M)\rangle$ can be naturally viewed as an array of M integers with the constraint $n_1 + n_2 + \cdots + n_M = N$. Taking a single species bosonic system, for instance, the coefficients of all $|\vec{n}\rangle$, e.g., $A_{\vec{n}}$ are normally stored in a one-dimensional array, and the index I, i.e., the position, of $A_{\vec{n}}$ in the array is given by an indexing function of $I(\vec{n})$. Due to the constraint of $n_1 + n_2 + \cdots + n_M = N$, we make use of the so-called Combinadic numbers[12,38] for the indexing. The Combinadic numbers can be characterized as follows: first, $\vec{n}$ is related to an integer $n_1 * N^{M-1} + \cdots + n_i * N^{M-i} + \cdots + n_M$, then all $\vec{n}$ are sorted by the descending order of this integer, and $I(\vec{n})$ is defined as the sequence number of $\vec{n}$ in the sequence. For example, we have $I[(N, 0, \ldots, 0)] = 1$, $I[(N-1, 1, 0, \ldots, 0)] = 2$ and $I[(0, \ldots, 0, N)] = \binom{N+M-1}{M-1}$. In the ML-MCTDHB implementation, the more important function is actually the inverse function of $I(\vec{n})$, named as $\vec{n}(I)$. We build a table T_1 of a $\binom{N+M-1}{M-1} \times M$ matrix to represent $\vec{n}(I)$, of which the element of $(T_1)_{ij}$ stores the occupation number in the jth orbital of the ith permanent state in the descending order. This table only needs to be built once at the beginning of the calculation with an overall negligible CPU time.

The second-quantization calculations mainly appear in the equations of motion for the species coefficients and also the mean-field operators of the particle layer. Here, we demonstrate the strategy applied in ML-MCTDHB for such second-quantization calculations with the example of the equations of motion. The equations of motion for $A_{\vec{n}}$ can be summarized as

$$i\,\partial_t A_{\vec{n}} = \sum_{i,j}\langle\vec{n}|\hat{H}_{1b}|\vec{n} + \hat{i} - \hat{j}\rangle A_{\vec{n}+\hat{i}-\hat{j}} + \sum_{i_1,i_2,j_1,j_2}\langle\vec{n}|\hat{H}_{2b}|\vec{n} + \hat{i}_1 + \hat{i}_2 - \hat{j}_1 - \hat{j}_2\rangle A_{\vec{n}+\hat{i}_1+\hat{i}_2-\hat{j}_1-\hat{j}_2}. \tag{36}$$

The first term on the rhs of the equation is related to the one-body operator, and the second term is related to the two-

body operator. Equation (36) must be applied to all permanent states. To calculate the rhs of (36), first we need to loop over all the permanent states of $\vec{n}$, and for each permanent state two more loops over the orbitals i, j, and i_1, i_2, j_1, j_2 are required for the one-body and two-body operators, which ends up with a loop of the total number $\binom{N+M-1}{M-1} * (M^2 + M^4)$. In each loop unit, the function $I(\vec{n} + \hat{i} - \hat{j})$ or $I(\vec{n} + \hat{i}_1 + \hat{i}_2 - \hat{j}_1 - \hat{j}_2)$ must be calculated, and this leads to huge numerical costs. The second quantization calculation for the mean-field operators are done in the same way as the equations of motion.

However, in the ML-MCTDHB implementation, we use another strategy which cannot only reduce the total amount of loops but meanwhile avoid the calculation of the index function $I(\vec{n} + \hat{i} - \hat{j})$ or $I(\vec{n} + \hat{i}_1 + \hat{i}_2 - \hat{j}_1 - \hat{j}_2)$. To illustrate this, we rewrite Eq. (36) as

$$\begin{aligned}\sum_{\vec{n}} (i\partial_t A_{\vec{n}})|\vec{n}\rangle = &\sum_{\vec{p}|N-1} \sum_{i,j} |\vec{p} + \hat{i}\rangle\langle\vec{p} + \hat{i}|\hat{H}_{1b}|\vec{p} + \hat{j}\rangle A_{\vec{p}+\hat{j}} \\ &+ \sum_{\vec{q}|N-2} \sum_{i_1,i_2,j_1,j_2} |\vec{q} + \hat{i}_1 + \hat{i}_2\rangle\langle\vec{q} + \hat{i}_1 \\ &+ \hat{i}_2|\hat{H}_{2b}|\vec{q} + \hat{j}_1 + \hat{j}_2\rangle A_{\vec{q}+\hat{j}_1+\hat{j}_2}. \end{aligned} \quad (37)$$

Equation (37) can be interpreted as follows: we generate a one-dimensional array of length $\binom{N+M-1}{M-1}$, which stores the value of $\partial_t A_{\vec{n}}$ for all the permanent states. To fill in the array, i.e., to calculate the time derivative of all the permanent states, we start with the one-body operators and loop over the permanent states $\vec{p}|N-1$ for $N-1$ bosons instead of those for N bosons and calculate $\langle\vec{p} + \hat{i}|\hat{H}_{1b}|\vec{p} + \hat{j}\rangle A_{\vec{p}+\hat{j}}$ to put the value in the position of $I(\vec{p} + \hat{i})$. For the two-body operators, we loop over the permanent states $\vec{p}|N-2$ for $N-2$ bosons, calculating $\langle\vec{q} + \hat{i}_1 + \hat{i}_2|\hat{H}_{2b}|\vec{q} + \hat{j}_1 + \hat{j}_2\rangle A_{\vec{q}+\hat{j}_1+\hat{j}_2}$ and putting it in the position $I(\vec{q} + \hat{i}_1 + \hat{i}_2)$ of the array. In this way, the total number of loops reduces from $\binom{N+M-1}{M-1} * (M^2 + M^4)$ to $\binom{N+M-2}{M-2} * M^2 + \binom{N+M-3}{M-3} * M^4$.

The strategy of Eq. (37) can also help to avoid calculating the indexing function $I(\vec{n})$, as $I(\vec{n})$ is only an intermediate step linking two permanent states, which can be done by means of two pre-build tables, named T_{1b} and T_{2b}, of $\binom{N+M-2}{M-2} * M$ and $\binom{N+M-3}{M-3} * M^2$ arrays, respectively. In T_{1b}, the element $(T_{1b})_{a,i}$ stores the index of the permanent state $I(\vec{p} + \hat{i})$, where the integer a is the Combinadic number of $|\vec{p}\rangle$. Similarly, the element $(T_{2b})_{a,i+(j-1)*M}$ stores the index of the permanent state $|\vec{p} + \hat{i} + \hat{j}\rangle$, with a being the Combinadic number of $|\vec{p}\rangle$. These two tables take almost negligible CPU time in the initialization step of the calculation. With Eq. (37), the total loops amount is greatly reduced and simultaneously the time-consuming calculations of the index functions is avoided, which leads to a great reduction of the CPU time of the overall calculations.

In this section, we have presented how we face the major challenge of the ML-MCTDHB implementation, namely, how to deal with the initialization and calculations within the second quantization formalism. We demonstrate that by introducing three indexing tables T_1, T_{1b}, and T_{2b}, we have an efficient solution to the difficulties in the second-quantization treatment, which both reduce the looping times and the calculation cost in each loop unit. Moreover, the T_{1b} and T_{2b} are particularly constructed for the one-body and two-body operators, and such a strategy also enables us to conveniently extend to F-particle interactions, simply by generating a table containing the mapping from permanent state $|\vec{p}\rangle$ to $|\vec{p} + \hat{i}_1 + \ldots + \hat{i}_F\rangle$.

B. ML-MCTDHB program

Having introduced the theory of ML-MCTDHB, we now turn to a brief introduction to our code. Our ML-MCTDHB code is based on the general ML-MCTDH implementation[9] in its recursive formulation.[8] We have developed our code based on the multilayer machinery of the Heidelberg MCTDH85 package,[39] and equipped it with the machinery of dealing with bosonic ensembles. Since this ML-MCTDH implementation is capable of handing arbitrary ML-MCTDH wave function expansions, we have extended the scheme to species and particle ML-MCTDHB as well as mixtures of both. Hence, in principle an arbitrary number of bosonic species in arbitrary dimensions can be treated.

As introduced in Sec. II, the ML-MCTDHB scheme is divided into various separate functional bricks, such as the initialization of the tree structure with the permanent tables T_1, T_{1b}, and T_{2b}, the construction of the Hamiltonian, the mean-field operators, and the density matrices of different layers, and the combination of all these components to the rhs of the equations of motion to perform the integration. Our ML-MCTDHB code is then designed in a systematic structure, consisting of various modules, which accommodate the requirements of different functional bricks of the method. The code can now carry out propagations in the real and imaginary time, which correspond to the calculation of the dynamics and the relaxation to the ground state, respectively. Moreover, improved relaxation[35] is also implemented in our code, in which the non-top node coefficients are still propagated in imaginary time while the top-node coefficients are obtained by direct diagonalization. In the improved relaxation, the imaginary time propagation of non-top node coefficients and the diagonalization of top node coefficients are done recursively. When convergence is reached, both the top-node and non-top node coefficients become constant in the diagonalization and imaginary time propagation, respectively, which corresponds to a stationary state of the system, i.e., an eigenstate. By carefully choosing the initial state of the improved relaxation, we can obtain different eigenstates of the system, which lie in the truncated Hilbert space given by the ML-MCTDHB *Ansatz*.

At the moment, our ML-MCTDHB scheme can deal with arbitrary two-body interactions – an extension to three- or four-body interactions would be straightforward. We adopt the product form of the interactions, as introduced in Sec. II A, and this allows a recursive construction of the Hamiltonian expressed and also the mean-field operators on different layers. Ultra-cold bosonic atoms constitute an important class of systems, which can be attacked by the ML-MCTDHB theory. In this particular context, the contact interaction turns out to be very relevant. Approximating the delta interaction potential by a narrow Gaussian, the POTFIT ma-

chinery can be applied for obtaining the desired product form (cf. Ref. 5). For one-dimensional settings, we have also developed an exact implementation of the contact interaction $V(x_1 - x_2) = g\,\delta(x_1 - x_2)$ *without* reshaping it into the product form in order to liberate the simulations from the artificial length scale induced by the Gaussian approximation of the delta function. Moreover, the direct implementation of the contact potential has speeded up the simulation by one order of magnitude in comparison to a product representation of the same accuracy. The main difference in the derivation of the equations of motion lies in the fact that one cannot separate the mean-field operators into a scalar matrix and a operator valued factor anymore, which breaks the recursive multi-layer formulation (cf. the Appendix). For the explicit equations of motion with the efficient treatment of the contact interaction, we refer the reader to Ref. 26.

Depending on the concrete problem, we employ an appropriate discrete variable representation (DVR) of the SPFs,[2,40] such as the (radial) harmonic oscillator DVR, the sine DVR, the exponential DVR, and the Legendre DVR, which have been implemented in our code. So in the case of the exact implementation of the delta interaction, the grid point spacing defines the smallest length scale, thus an ultraviolet cutoff.

For integrating the equations of motion, we employ either ZVODE, a variable-coefficient ordinary differential equation solver with fixed-leading-coefficient implementation,[41] or DOPRI, an explicit Runge-Kutta method of order five with step size control and dense output.[42]

We can also use the ML-MCTDHB scheme to calculate the expectation values of the combination of one-body and two-body operators. For instance, we can calculate the total energy or separately the kinetic energy and potential energy evolution, the one-body density and the two-body density matrices. Especially, the two-body density matrices are already calculated during the propagation as a building brick for the mean-field operators, so that such quantities can be obtained for free in terms of computational time (cf. also Ref. 43).

IV. APPLICATIONS

In the following, we focus on the tunneling dynamics of ultra-cold bosonic atoms in a one-dimensional double well trap made of a harmonic trap superimposed with a Gaussian at the trap centre, i.e., $V_{trap}(x) = x^2/2 + h/\sqrt{2\pi s^2} * \exp(-x^2/2s^2)$ in harmonic oscillator units $\hbar = m = \omega = 1$. First, we will compare the single species tunneling results of our ML-MCTDHB implementation with the results of the implementations of MCTDH.[39] Then we apply species ML-MCTDHB to simulate the tunneling of a bosonic mixture and compare the results to the ML-MCTDH simulations.[9] Applications of particle ML-MCTDHB will be presented somewhere else.

In both examples, we prepare the initial state by modifying the trapping potential such that it becomes energetically favorable for the bosons to be in the left well. The bosonic ensemble is then relaxed to the many-body ground state by propagating the equations of motion in imaginary time. The resulting many-body state is finally propagated in real time in the original double well trap.

A. Single-species tunneling

As a first application, we simulate the tunneling dynamics of a single-species bosonic ensemble in the double well. The tunneling dynamics of a bosonic ensemble in a one-dimensional double well has been extensively studied, for both microscopic and macroscopic systems, with boson numbers ranging from two to the order of 10^6 and even more.[5,18,44–47] Experiments on the double-well tunneling have also been carried out.[48–50] Various theoretical approaches have been employed, for instance, the Gross-Pitaevskii equation,[44,45] the Bose-Hubbard model,[46,47] as well as *ab initio* methods: MCTDHB has been applied to the many-body system,[18] and calculations via MCTDH have been carried out for few-body systems.[5] The simulations based on the single-band approximation predict that the tunneling is suppressed for interaction strengths above some critical value, while the extended model predicts the weakening of such a suppression in the strong interaction regime, where higher bands effects cannot be neglected. In this way, the double well potential manifests itself as a proper test bed for the higher band effects. In this section, we will simulate the double well tunneling with ML-MCTDHB, and perform a detailed analysis to resolve the higher bands effects.

Here, we present the tunneling dynamics of four and ten bosons in a double well potential. A sin-DVR is employed, which intrinsically introduces hard-wall boundaries at both ends of the potential (cf. Appendix of Ref. 2). First, we show the simulation of the four-boson tunneling, in comparison with the MCTDH simulation using the Heidelberg MCTDH package.[39] To have a direct comparison between ML-MCTDHB and MCTDH results, we adopt in both simulations a narrow Gaussian interaction to model the contact interaction, and the interaction is written as $V(x_1 - x_2) = g(2\pi\sigma^2)^{-1/2}\exp(-(x_1 - x_2)^2/(2\sigma^2))$, with $\sigma = 0.05$. Next, we extend the simulation to the ten-boson case, and the contact interaction is modeled by the exact delta function. The simulation of the tunneling of ten bosons becomes impractical with MCTDH, and we only perform the simulation with ML-MCTDHB.

Figure 4 summarizes the population evolution of 4 bosons in the double well for different interaction strengths. When the interaction strength is zero, the system undergoes Rabi oscillations, as shown in Figure 4(a). As the interaction strength increases to 0.5, the oscillations almost vanish on a relative long time scale, which indicates the delayed tunneling behavior. When the interaction strength increases to 2.0, as shown in Figure 4(c), the amplitude of the population oscillations is increased from less than 0.06 in delayed tunneling (Figure 4(b)) to around 1.0, which is referred to as enhanced tunneling. As the interaction increases even further to 4.0, the quasistationary state is approached during tunneling, where the populations of the left and the right well approach the value of two with only small fluctuations, as shown in Figure 4(d). Summarizing, Figure 4 illustrates the tunneling transition from Rabi oscillations through delayed tun-

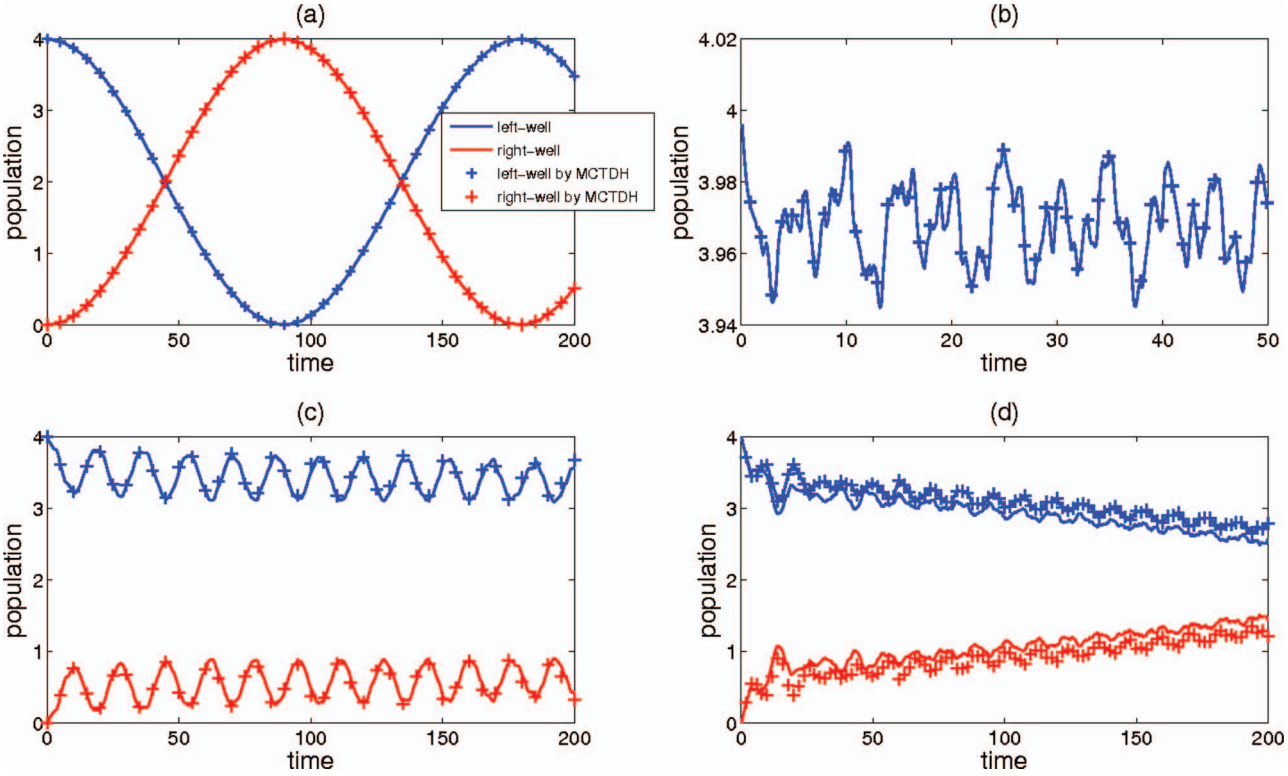

FIG. 4. The population oscillation of four bosons in the left and right well, with (a) g = 0.0, (b) g = 0.5, (c) g = 2.0, and (d) g = 4.0. Lines: ML-MCTDHB results. Crosses: MCTDH results. Figures 4(a)–4(c): Six particle SPFs; Figure 4(d): Ten particle SPFs. Particularly, Figure 4(b) shows the behavior for a shorter time interval to highlight the agreement between the two methods concerning the fast oscillation process. The difference between the two methods in Figure 4(d) is attributed to the different implementations of the contact interaction in the two methods (cf. main text).

neling and enhanced tunneling to the quasistationary state as the interaction strength increases from zero to the strong interaction regime. The ML-MCTDHB results show a very good agreement with the MCTDH calculations. Only for the interaction strength $g = 4.0$, deviations occur, which can be explained by the different implementations of the POTFIT algorithm in MCTDH and ML-MCTDHB. Nevertheless, we still observe qualitatively the same behavior of the emergence of the quasistationary state in both simulations. Moreover, more orbitals are needed to achieve good convergence in the strong interaction case of $g = 4.0$, and we supply ten orbitals to this case, where good convergence can be deduced from the natural populations discussed in the following.

The natural populations can confirm the convergence of the calculation and also manifest themselves as a measure of the fragmentation of the system,[51] which is defined as the depletion of the population of the highest occupied natural orbital from unity. To uncover the fundamental effect giving rise to the enhanced tunneling and quasistationary state, we plot the natural populations and one-body density profiles of the four-boson ensemble at different time instants during the tunneling process in Figures 5. Figure 5(a) and 5(c) show the natural populations and one-body densities for $g = 2.0$. In Figure 5(a), first we see the lowest natural population saturates to a value less than 10^{-3}, which confirms the convergence of the simulation. In Figure 5(c), we observe that the profile in the left well remains as a Gaussian packet, while the profile in the right well presents a two-hump structure. The two-hump profile is a signature of the occupation of the first excited state in the right well, and this indicates that the enhanced tunneling is due to the higher band occupation, i.e., the interband tunneling. In the 2-boson ensemble,[5] the enhanced tunneling only takes place in the fermionization regime, i.e., for the interaction strength approaching infinity, while as the number of bosons increases, it becomes easier to excite higher bands, and the enhanced tunneling arises even in an interaction regime far below the fermionization limit.

The natural populations for $g = 4.0$, as shown in Figure 5(b) show a good convergence of the simulation with the lowest natural population saturating well below 1%, and at $g = 4.0$ more natural orbitals contribute to the tunneling process, which suggests that fragmentation of the system and the presence of multiple tunneling channels in the dynamics. Figure 5(d) shows the one-body densities at different times for the interaction strength $g = 4.0$, where the quasistationary state dominates the tunneling. During the tunneling, the one-body density profile presents multiple oscillations in both the left and right wells, which indicates multiple higher-band excitations in the tunneling process. In the exact quantum dynamics study of the double well system,[18] the quasistationary state is explained by the quick loss of coherence of the system, and the multiple excitation of higher energetic levels in the left and right well suggests that the tunneling process involves a large number of higher band number states, and in consequence multiple tunneling channels. The dephasing between these tunneling channels can be a source of the loss of coherence of the bosons in the two wells.

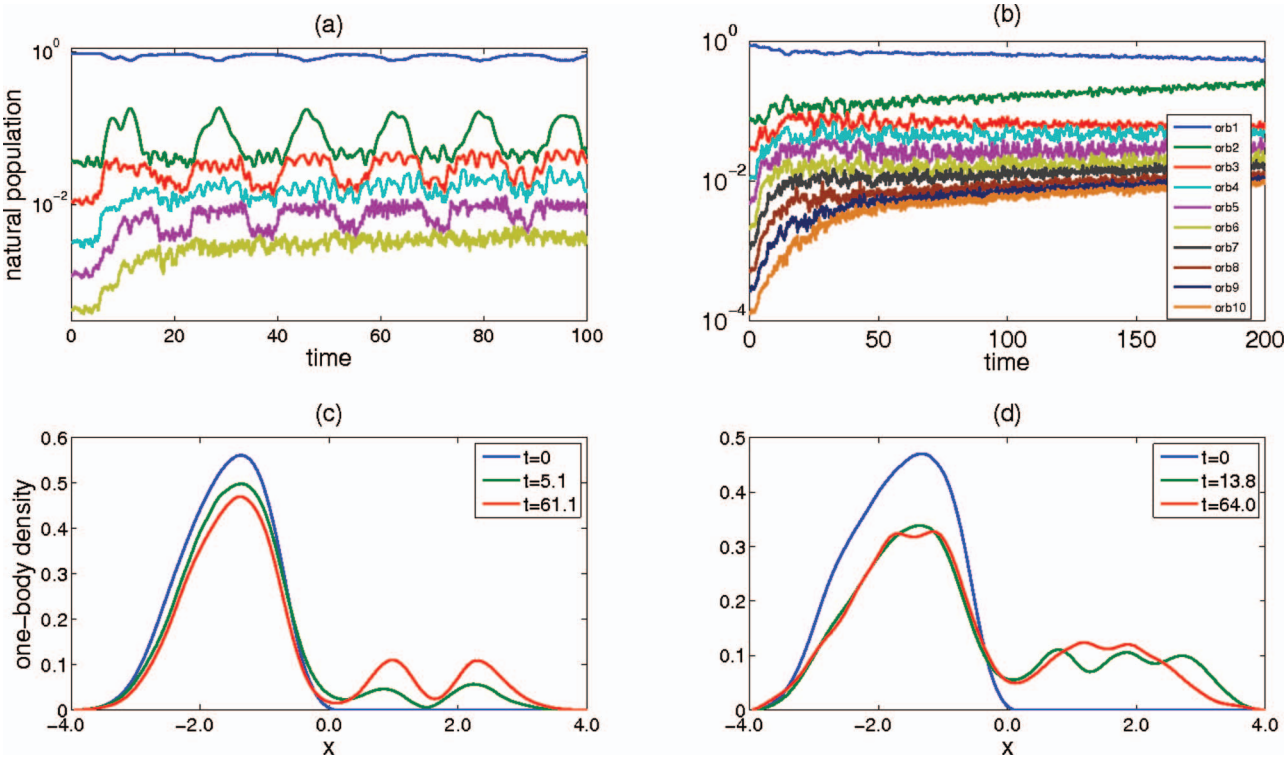

FIG. 5. The natural populations and one-body densities of the system of four bosons in the double well at different time instants, with (a) and (c) for g = 2.0, as well as (b) and (d) for g = 4.0.

Figure 6 shows the tunneling evolution of a system of ten bosons in the double well with varying interaction strength. We focus on the enhanced tunneling and quasistationary state for a sufficiently large interaction strength. Enhanced tunneling is observed with an interaction strength as weak as $g = 0.5$, as shown in Figure 6, and at $g = 1.0$ the system slowly evolves to the quasistationary state. Figures 7(a)–7(d) show the natural populations and one-body densities at different time instants during the tunneling process of Figures 6(a) and 6(b), respectively. The fact that the lowest natural population saturates to relatively small values of the order of 0.1% and 1% in Figures 7(a) and 7(b), respectively, illustrates the well-controlled behavior of the convergence of the simulation. In Figure 7(c), the two-hump profile in the right well indicates that the enhanced tunneling is again a result of interband tunneling, and the multi-mode oscillatory structure in Figure 7(d) suggests that multiple tunneling channels are involved and this can lead to the decoherence between the two wells, and consequently to the appearance of the quasistationary state.

To summarize, in this section we presented the tunneling dynamics of single species bosons in a one-dimensional double well potential. We supply the cross-check with results obtained by the Heidelberg MCTDH, which indicates the

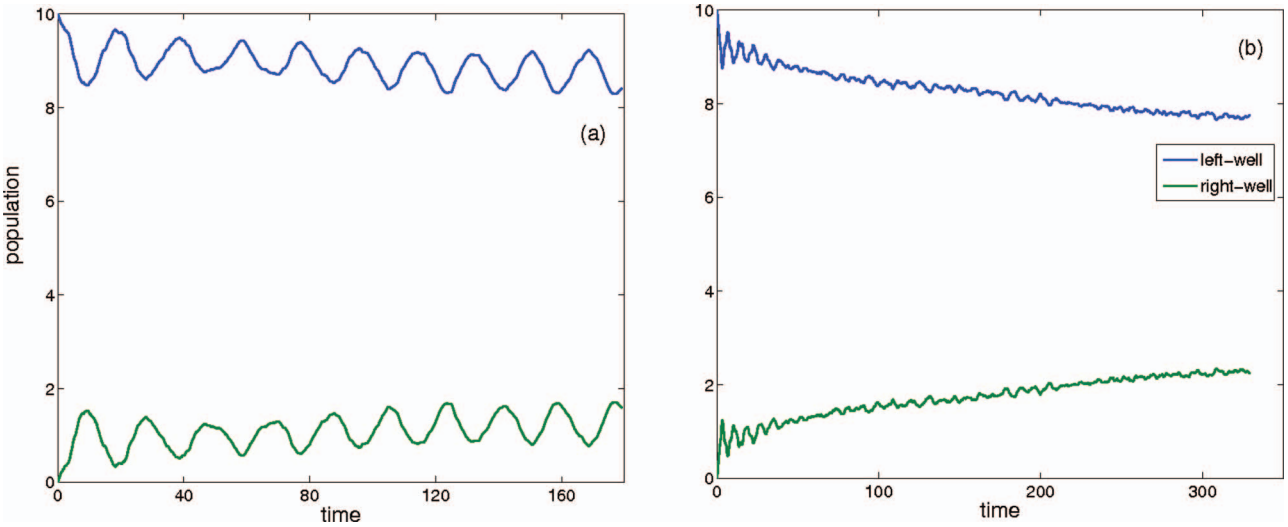

FIG. 6. The population oscillation of ten bosons in the double well, with (a) g = 0.5, (b) g = 1.0. Enhanced tunneling is obtained in (a), where the amplitude of the population is around 2. A slow evolution to the quasistationary state is obtained in (b).

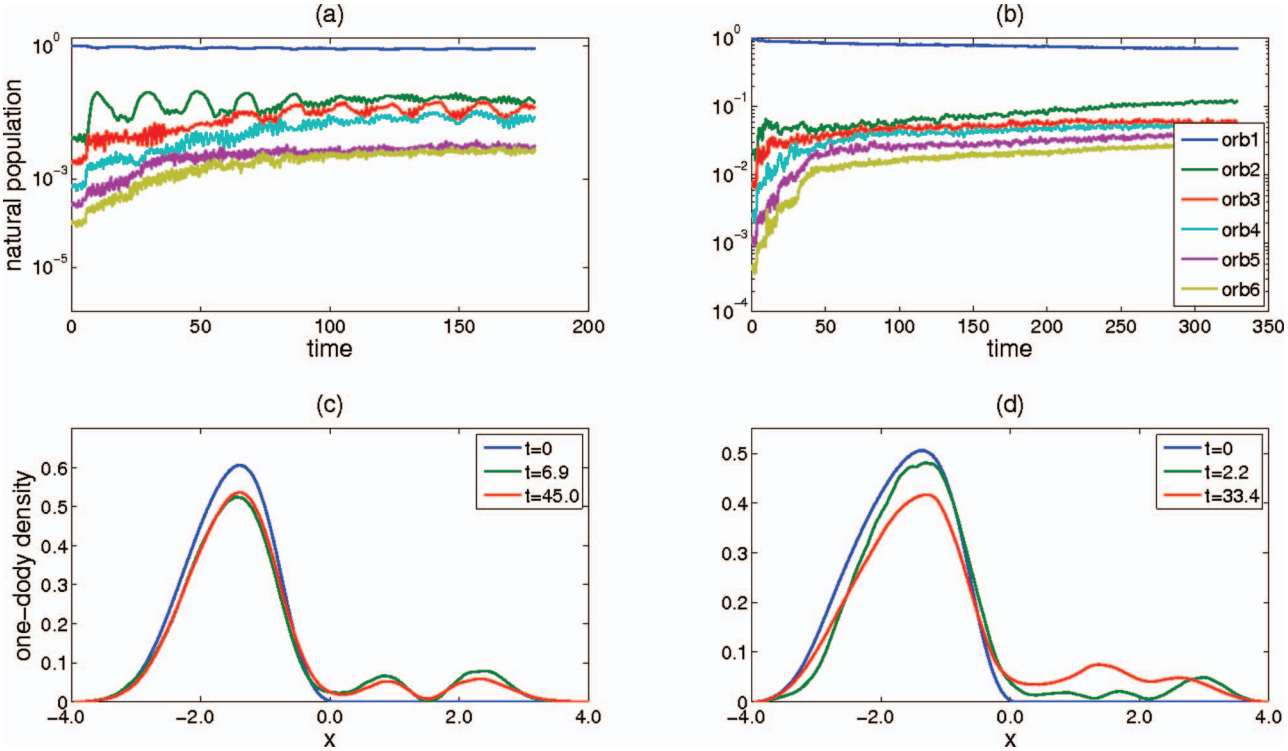

FIG. 7. The natural population and one-body densities of ten bosons in the double well at different time, with (a) and (c) g = 2.0, as well as (b) and (d) g = 4.0.

stable performance of ML-MCTDHB, and also the check of convergence by the natural populations. Further, we also demonstrate the ability of the method for various and extended investigations, via different analysis routines, such as the population evolution and the one-body density evolution for larger systems.

B. Mixture tunneling

Let us now consider the tunneling dynamics of two bosonic species, called the A and B species which are loaded in the left well of the double well trap. All species shall have the same mass, which is set to one, and shall experience the same double well potential $V_{trap}(x)$. The intra-species interaction strengths g_σ of the contact interaction potentials $V_\sigma(x) = g_\sigma \delta(x)$ ($\sigma = A, B$), however, are assumed to be different for different species σ. Furthermore, the inter-species interaction is also modeled by a pseudo-potential: $V_{AB}(x_A - x_B) = g_{AB}\delta(x_A - x_B)$. All delta potentials are implemented numerically exactly as explained in Ref. 26. The choice $h = 3$ and $s = 0.2$ provides us with three bands below the barrier energy with two single particle eigenstates each. The energetic separation of the lowest band to the first one amounts to 1.63, while the level spacing of the lowest band equals 0.23 resulting in a Rabi-tunneling period of 27. For preparing the initial state of the mixture, we modify the double well trap by letting $V_{trap}(x) = 20.0$ for $x > 0$.

We consider a binary mixture made of 2 A and 2 B bosons. With $g_A = 0.3$, $g_B = 0.5\, g_A$, and $g_{AB} = 0.1\, g_A$. Due to the not too different intra-species interaction strengths, we provide for each species the same number of species SPFs, $M_\sigma \equiv M = 4$, and particle SPFs, $m_\sigma \equiv m = 3$. In the following, we compare simulations done with ML-MCTDHB and ML-MCTDH.[9] Although the initial state for the relaxation run is – from a mathematical perspective – perfectly symmetric with respect to particle exchange within each species, one has to pay attention to the initially unoccupied species SPFs in ML-MCTDH. These have to be symmetrized "by hand" because otherwise the ML-MCTDH propagation will not preserve the exchange symmetry within each species.

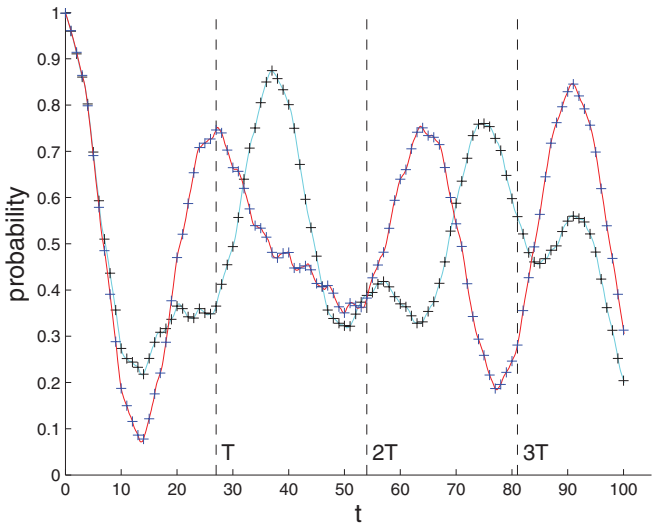

FIG. 8. 2 A and 2 B bosons initially loaded in the left well of a double well trap. Blue (red) line: Probability for finding an A (B) boson in the left well versus time. Line: ML-MCTDHB results. Crosses via ML-MCTDH. Parameters: $g_A = 0.3$, $g_B = 0.5\, g_A$, and $g_{AB} = 0.1\, g_A$. $M = 4$ and $m = 3$ SPFs for both calculations. The dashed vertical lines: the first three Rabi-tunneling periods of a single particle.

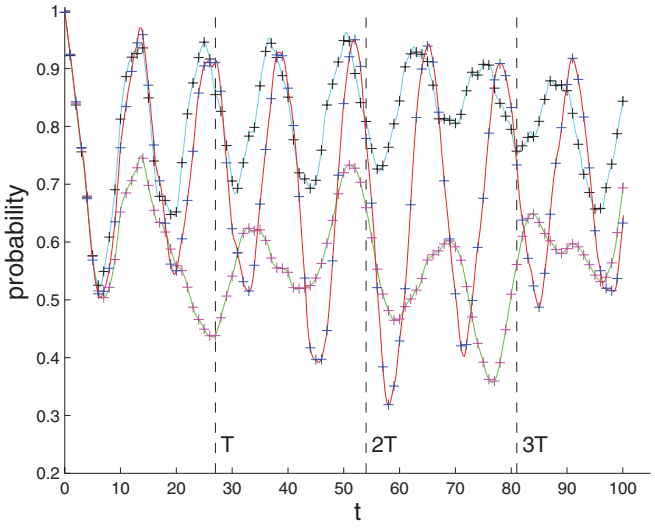

FIG. 9. Evolution of several joint probabilities for the same setup as in Figure 8: The blue (red) solid line: probability of finding both A (B) bosons in the same well; The green solid line: The probability of detecting an A and a B boson in the same well. Solid lines: ML-MCTDHB. Crosses: ML-MCTDH. Dashed vertical lines: The first three Rabi-tunneling periods.

MCTDH and its derivative methods are proven to preserve both the norm and the total energy exactly (cf. Appendix of Ref. 2). Using the ZVODE integrator with an absolute and relative tolerance of 10^{-10} and integrating 100 harmonic oscillator time units, the norm of the total wave function deviates from unity by 10^{-7} and the total energy is conserved up to 10^{-6} for both ML-MCTDH and ML-MCTDHB.

Before discussing the convergence of the simulations with respect to the number of particle and species SPFs, we first summarize the results for the different one- and two-body observables. Figure 8 shows the time evolution of the probability for finding an A (B) boson in the left well. One clearly sees that the tunneling period of the A bosons is enlarged in comparison to the Rabi-tunneling period. In contrast to this, the probability evolution of finding a B boson in the left well qualitatively resembles a first Rabi-cycle but afterwards also features a delay. This observation is quite plausible: Since both the g_B and g_{AB} are smaller than g_A, one expects that the B bosons require a longer interaction time in order to show an interaction-induced effect. The impact of the different interaction strengths can also be seen in Figure 9: While the probability for finding two A bosons in the same well is well above 0.5 for most of the propagation time, showing a binding tendency, the B bosons tend to stay in the same well less likely. On the contrary, the probability for finding an A and a B boson in the same well fluctuates around 0.5 indicating that the bosons of each species tunnel independently.

For judging the convergence of the simulations, we present the natural populations for different subsystems. Figure 10 shows the natural populations corresponding to the reduced density matrix of the whole species A (or B). One

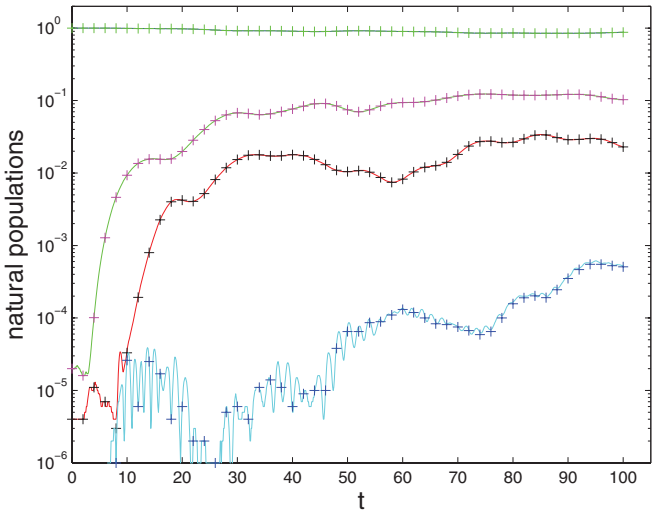

FIG. 10. The natural populations, i.e., eigenvalues of the reduced density matrix corresponding to the whole species A (or equivalently B) are plotted versus time for the same tunneling scenario as in Figure 8. The solid lines refer to the ML-MCTDHB and the crosses to the corresponding ML-MCTDH calculation.

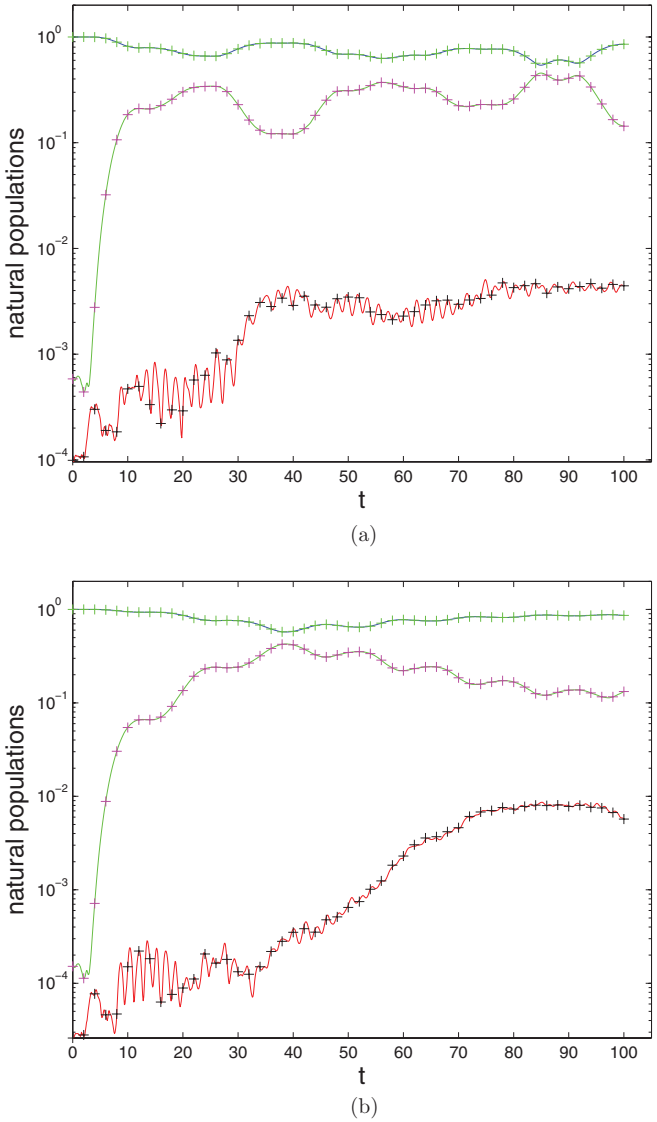

FIG. 11. The dynamics of the natural populations of the reduced density matrix corresponding to an A and a B boson are shown in (a) and (b), respectively. All parameters are chosen as in Figure 8. The solid lines: ML-MCTDHB; the crosses: ML-MCTDH calculation.

clearly sees that after about 25 time units three species states contribute to the total wave function with weights of the order of 89%, 10%, and 1%. The fourth state contributes so little that it could be neglected without affecting the results. The natural populations of the reduced density matrix corresponding to an A and a B boson, respectively, are plotted in Figure 11. Here again, we notice that the lowest natural population stays well below 1%, meaning that its natural orbital, the corresponding eigenstate of the respective reduced one-body density matrix, has only marginal influence on the result. Furthermore, we observe that two natural orbitals contribute with almost equal weight during certain time intervals. Hence, a mean-field approximation would be improper, which was to be expected for such a few-body system. In terms of the numerical correctness of our implementation, we note that the ML-MCTDHB results excellently agree with the simulations performed with ML-MCTDH.

In this section, we have demonstrated the correctness of the implementation of ML-MCTDHB in comparison with MCTDH and ML-MCTDH, with an excellent agreement being observed. It is worth pointing out that ML-MCTDHB is not only more efficient, but allows us to treat more complicated systems with more particles, more species, and for stronger correlations. For an application of ML-MCTDHB to a more involved tunneling scenario of a bosonic mixture, we refer the reader to Ref. 26.

V. CONCLUSIONS AND OUTLOOK

The *ab initio* methods MCTDHB and ML-MCTDH for the investigation of many-particle quantum systems possess different emphases and foci: While MCTDHB aims at employing the bosonic particle exchange symmetry for obtaining a better performance, ML-MCTDH focuses on how to obtain a more compact *Ansatz* for the many-body wave function by employing physical knowledge about correlations within and between *subsystems*. In general, however, the high flexibility of the ML-MCTDH wave function *Ansatz* is incompatible with the generic correlations due to the bosonic exchange symmetry in a MCTDHB wave function expansion.

In this work, we have shown that one can benefit from the advantages of both the MCTDHB and the ML-MCTDH concept if one restricts oneself to two – quite natural – classes of wave function expansion schemes (and any combination thereof): (i) In species ML-MCTDHB, the total wave function of a bosonic multi-component system first is expanded in Hartree products made of states with each of them corresponding to a state of a whole species. Then each of these species states is expanded in permanents like in MCTDHB. (ii) In particle ML-MCTDHB, a single component bosonic system is considered with the bosons living in two or three dimensions and/or having internal degrees of freedom. There, the total wave function is expanded in terms of permanents and a ML-MCTDH expansion is applied to all the orbitals underlying those permanents. Summarizing, the bosonic exchange symmetry is exactly and efficiently taken into account in ML-MCTDHB as any state of indistinguishable bosons is expanded in permanents. The multi-layer concept is then employed for obtaining an optimized wave function *Ansatz* guided by the correlations between different species (intra- versus inter-species correlations) or between different spatial directions (e.g., in quasi two- or quasi-three-dimensional systems) or internal degrees of freedom. By comparing with other methods of the MCTDH family, we have demonstrated the beneficial scaling of ML-MCTDHB. Like in all MCTDH type methods, the convergence of a simulation with respect to the number of provided states in the wave function *Ansatz* can be judged by the eigenvalue distributions of the reduced density matrices corresponding to different subsystems.

We have implemented ML-MCTDHB on the basis of the ML-MCTDH scheme[9,39] in such a general way that, in principle, we can deal with an arbitrary number of species in arbitrary dimensions with different types of interactions, such as the contact as well as the dipolar interactions – only limited by the number of states needed for a converged simulation, which depends on the system details, of course. Furthermore, the scheme can in principle also deal with hybrid systems such as a single ion coupled to an environment of indistinguishable bosons like liquid ^{4}He as long as all the interactions can be efficiently brought into the POTFIT product form.

Finally, we note that both conceptually and practically it is relatively straightforward to generalize the presented method to fermionic systems, i.e., to ML-MCTDHF, or to mixed bosonic-fermionic systems, i.e., to ML-MCTDHBF: Similar to Eq. (4), one could start with an appropriate ML-MCTDH expansion in which all indistinguishable particles of one kind are grouped into a species node, and expand the species SPFs with respect to the permanent states and slater determinants for bosonic and fermionic species, respectively. This approach is in particular compatible with our ML-MCTDHB method and its implementation, and would lead to a highly efficient algorithm for simulating the most general composite systems consisting of subsystems with indistinguishable constituents.

ACKNOWLEDGMENTS

The authors would like to thank Hans-Dieter Meyer and Jan Stockhofe for fruitful discussions on MCTDH methods and symmetry conservation. Particularly, the authors would like to thank Jan Stockhofe for the DVR implementation of the ML-MCTDHB code. We also thank Johannes Schurer and Valentin Bolsinger for carefully reading the manuscript. S.K. gratefully acknowledges a scholarship of the Studienstiftung des deutschen Volkes. L.C. and P.S. gratefully acknowledge funding by the Deutsche Forschungsgemeinschaft (DFG) in the framework of the SFB 925 "Light induced dynamics and control of correlated quantum systems."

APPENDIX: SPECIES MULTI-LAYER MCTDHB EQUATIONS OF MOTION WITHOUT PRODUCT FORM OF THE HAMILTONIAN

Here, we provide the explicit equations of motion without using the product form of the interactions. We first introduce

the Hamiltonian in the second quantization picture, as

$$H = \sum_{\kappa}\sum_{i,j}\left(H_0^{3;\kappa}\right)_{ij}\hat{a}^{\dagger}_{\kappa,i}\hat{a}_{\kappa,j} + \frac{1}{2}\sum_{\kappa}\sum_{i_1,i_2,j_1,j_2}(V^{3;\kappa})_{i_1i_2j_1j_2}\hat{a}^{\dagger}_{\kappa,i_1}\hat{a}^{\dagger}_{\kappa,i_2}\hat{a}_{\kappa,j_1}\hat{a}_{\kappa,j_2} + \sum_{\kappa_1<\kappa_2}\sum_{i_1,i_2,j_1,j_2}(W^{3;\kappa_1,\kappa_2})_{i_1i_2j_1j_2}\hat{a}^{\dagger}_{\kappa_1,i_1}\hat{a}^{\dagger}_{\kappa_2,i_2}\hat{a}_{\kappa_1,j_1}\hat{a}_{\kappa_2,j_2}. \tag{A1}$$

$\hat{a}_{\kappa,i}$ ($\hat{a}^{\dagger}_{\kappa,i}$) refers to the operator annihilating (creating) a κ boson in the SPF state $|\phi_i^{3;\kappa}\rangle$. The coefficients in the Hamiltonian terms are $(H_0^{3;\kappa})_{ij} = \langle\phi_i^{3;\kappa}|\hat{H}_{\kappa}^0|\phi_j^{3;\kappa}\rangle$, $(V^{3;\kappa})_{i_1i_2j_1j_2} = \langle\phi_{i_1}^{3;\kappa}|\langle\phi_{i_2}^{3;\kappa}|\hat{V}|\phi_{j_1}^{3;\kappa}\rangle|\phi_{j_2}^{3;\kappa}\rangle$, and $(W^{3;\kappa_1,\kappa_2})_{i_1i_2j_1j_2} = \langle\phi_{i_1}^{3;\kappa_1}|\langle\phi_{i_2}^{3;\kappa_2}|\hat{W}^{\kappa_1,\kappa_2}|\phi_{j_1}^{3;\kappa_1}\rangle|\phi_{j_2}^{3;\kappa_2}\rangle$. The equations of motion (12) and (13) can be simplified as follows:

$$i\partial_t A_I^1 = \sum_{\kappa}\sum_{j}\left[\sum_{p,q}\left(H_0^{3;\kappa}\right)_{pq}\left(\tilde{Q}_{pq}^{\kappa}\right)_{i_\kappa j} + \frac{1}{2}\sum_{p_1,p_2,q_1,q_2}(V^{3;\kappa})_{p_1p_2q_1q_2}\left(\tilde{P}^{\kappa}_{p_1p_2q_1q_2}\right)_{i_\kappa j}\right]A^1_{I_j^{\kappa}} + \sum_{\kappa_1<\kappa_2}\sum_{j_1,j_2}\left[\sum_{p_1,p_2,q_1,q_2}(W^{3;\kappa_1,\kappa_2})_{p_1,p_2,q_1,q_2} \times \left(\tilde{Q}^{\kappa_1}_{p_1q_1}\right)_{i_1j_1}\left(\tilde{Q}^{\kappa_2}_{p_2q_2}\right)_{i_2j_2}\right]A^1_{I_{j_1j_2}^{\kappa_1\kappa_2}}. \tag{A2}$$

I is again defined as an array $(i_1, i_2, \ldots, i_S)$, while I_j^{κ} and $I_{j_1j_2}^{\kappa_1\kappa_2}$ are the arrays obtained by replacing i_κ in I by j and i_{κ_1}, i_{κ_2} by j_1, j_2 in I, respectively.

On the species layer, the Hamiltonian terms with nontrivial contribution to the rhs of Eq. (13) for $A^{2;\kappa}_{i;\vec{n}}$ are single particle Hamiltonian and intraspecies interaction terms of the κ species as well as the interspecies interaction terms between the κ species and other species, while the remaining Hamiltonian terms do not contribute to the rhs due to the projection operator. The equations of motion on the species layer can be obtained by substituting the corresponding inverse density matrices and the mean-field operators $\langle\hat{H}\rangle^{2;\kappa}_{i,j}$ to Eq. (13). The density matrices are calculated in the same way as in Sec. II A 2, and the mean-field operator $\langle\hat{H}\rangle^{2;\kappa}_{i,j}$, keeping only the nontrivial terms, is $\langle\hat{H}_{\kappa}^0 + \hat{V}\rangle^{2;\kappa}_{i,j} + \langle\hat{W}_{\kappa}\rangle^{2;\kappa}_{i,j}$, and the mean-field operator for single particle Hamiltonian and intraspecies interaction terms are calculated as

$$\left\langle\hat{H}_{\kappa}^0 + \hat{V}_{\kappa}\right\rangle^{2;\kappa}_{i,j} = (\rho^{2;\kappa})_{ij} * \left(\hat{H}_0^{3;\kappa} + \hat{V}^{3;\kappa}\right). \tag{A3}$$

The mean-field operator for interspecies interaction is defined as $\langle\hat{W}_{\kappa}\rangle^{2;\kappa}_{i,j} \equiv \sum_{\nu\neq\kappa}\langle\hat{W}_{\kappa}\rangle^{2;\kappa,\nu}_{i,j}$, with

$$\langle\hat{W}\rangle^{2;\kappa,\nu}_{ij} = \sum_{\vec{n}|N_{\kappa}-1}\sum_{p,q=1}^{m_{\kappa}}Q_{\vec{n}}(p,q)|\vec{n}+\hat{p}\rangle_{\kappa}\langle\vec{n}+\hat{q}| \times\left[\sum_{r_{\kappa}=1}^{\mathscr{M}_{\kappa}}\left(A^{3;\kappa}_{p;r^{\kappa}}\right)^{*}A^{3;\kappa}_{q;r^{\kappa}}\left(W_{ij}^{\kappa,\nu}\right)(r^{\kappa})\right],$$
$$(W_{ij}^{\kappa,\nu})(r^{\kappa}) = \sum_{I^{\kappa\nu}}\sum_{r,s=1}^{M_{\nu}}\left(A^1_{I^{\kappa\nu}_{ir}}\right)^{*}A^1_{I^{\kappa\nu}_{js}}\sum_{p,q=1}^{m_{\mu}}\left(\tilde{Q}^{\nu}_{pq}\right)_{rs} \times\sum_{l_{\nu}=1}^{\mathscr{M}_{\nu}}\left(A^{3;\nu}_{p;l^{\nu}}\right)^{*}A^{3;\nu}_{q;l^{\nu}}W_{\kappa,\nu}(r^{\kappa},l^{\nu}). \tag{A4}$$

The equations of motion for the particle layer are then obtained by substituting the corresponding inverse density matrix and mean-field operators to Eq. (13). The mean-field operators for the single particle Hamiltonian, intraspecies and interspecies interactions are obtained as

$$\left\langle\hat{H}_{\kappa}^0\right\rangle^{3;\kappa}_{kj} = \rho^{3;\kappa}_{ij} * \hat{H}^0_{\kappa},$$
$$\left\langle\hat{V}_{\kappa}\right\rangle^{3;\kappa}_{kj} = \frac{1}{N_{\kappa}}\sum_{r^{\kappa}}\left(V^{\kappa}_{kj}\right)(r^{\kappa})|r^{\kappa}\rangle\langle r^{\kappa}|,$$
$$\left\langle\hat{W}_{\kappa,\nu}\right\rangle^{3;\kappa}_{kj} = \frac{1}{N_{\kappa}}\sum_{r^{\kappa}}\left[\sum_{rs}\left(\tilde{Q}^{\kappa}_{kj}\right)_{rs}\left(W^{\kappa,\nu}_{rs}\right)(r^{\kappa})\right]|r^{\kappa}\rangle\langle r^{\kappa}|. \tag{A5}$$

$(V^{\kappa}_{kj})(r^{\kappa})$ takes on the following appearance:

$$\left(V^{\kappa}_{kj}\right)(r^{\kappa}) = \sum_{rs}(\rho^{2;\kappa})_{rs}\left\{\sum_{pq}\left(\tilde{P}^{\kappa}_{kpjq}\right)_{rs} \times\left[\sum_{l}V_{\kappa}(r^{\kappa},l)\left(A^{3;\kappa}_{p;l}\right)^{*}A^{3;\kappa}_{q;l}\right]\right\}. \tag{A6}$$

[1] H.-D. Meyer, U. Manthe, and L. S. Cederbaum, Chem. Phys. Lett. **165**, 73 (1990).
[2] M. H. Beck, A. Jäckle, G. A. Worth, and H.-D. Meyer, Phys. Rep. **324**, 1 (2000).
[3] H.-D. Meyer, WIREs Comput. Mol. Sci. **2**, 351 (2012).
[4] *Multidimensional Quantum Dynamics: MCTDH Theory and Applications*, edited by H.-D. Meyer, F. Gatti, and G. A. Worth (Wiley-VCH, 2009).
[5] S. Zöllner, H.-D. Meyer, and P. Schmelcher, Phys. Rev. Lett. **100**, 040401 (2008).
[6] L. Cao, I. Brouzos, S. Zöllner, and P. Schmelcher, New J. Phys. **13**, 033032 (2011).
[7] H. Wang and M. Thoss, J. Chem. Phys. **119**, 1289 (2003).
[8] U. Manthe, J. Chem. Phys. **128**, 164116 (2008).
[9] O. Vendrell and H.-D. Meyer, J. Chem. Phys. **134**, 044135 (2011).
[10] A. I. Streltsov, O. E. Alon, and L. S. Cederbaum, Phys. Rev. Lett. **99**, 030402 (2007).
[11] O. E. Alon, A. I. Streltsov, and L. S. Cederbaum, Phys. Rev. A **77**, 033613 (2008).
[12] A. I. Streltsov, O. E. Alon, and L. S. Cederbaum, Phys. Rev. A **81**, 022124 (2010).
[13] J. Zanghellini, M. Kitzler, C. Fabian, T. Brabec, and A. Scrinzi, Laser Phys. **13**, 1064 (2003).
[14] G. Jordan, J. Caillat, C. Ede, and A. Scrinzi, J. Phys. B **39**, S341 (2006).

[15]M. Nest, R. Padmanaban, and P. Saalfrank, J. Chem. Phys. **126**, 214106 (2007).
[16]D. Hochstuhl and M. Bonitz, J. Chem. Phys. **134**, 084106 (2011).
[17]D. J. Haxton, K. V. Lawler, and C. W. McCurdy, Phys. Rev. A **86**, 013406 (2012).
[18]K. Sakmann, A. I. Streltsov, O. E. Alon, and L. S. Cederbaum, Phys. Rev. Lett. **103**, 220601 (2009).
[19]A. I. Streltsov, O. E. Alon, and L. S. Cederbaum, Phys. Rev. Lett. **106**, 240401 (2011).
[20]O. E. Alon, A. I. Streltsov, and L. S. Cederbaum, Phys. Rev. A **76**, 062501 (2007).
[21]O. E. Alon, A. I. Streltsov, K. Sakmann, A. U. J. Lode, J. Grond, and L. S. Cederbaum, Chem. Phys. **401**, 2 (2012).
[22]O. E. Alon, A. I. Streltsov, and L. S. Cederbaum, Phys. Rev. A **79**, 022503 (2009).
[23]H. Wang and M. Thoss, J. Chem. Phys. **131**, 024114 (2009).
[24]H. Wang, I. Pshenichnyuk, R. Härtle, and M. Thoss, J. Chem. Phys. **135**, 244506 (2011).
[25]K. F. Albrecht, H. Wang, L. Mühlbacher, M. Thoss, and A. Komnik, Phys. Rev. B **86**, 081412 (2012).
[26]S. Krönke, L. Cao, O. Vendrell, and P. Schmelcher, New J. Phys. **15**, 063018 (2013).
[27]G. Modugno, M. Modugno, F. Riboli, G. Roati, and M. Inguscio, Phys. Rev. Lett. **89**, 190404 (2002).
[28]P. Soltan-Panahi, J. Struck, P. Hauke, A. Bick, W. Plenkers, G. Meineke, C. Becker, P. Windpassinger, M. Lewenstein, and K. Sengstock, Nat. Phys. **7**, 434 (2011).
[29]P. Soltan-Panahi, D.-S. Lühmann, J. Struck, P. Windpassinger, and K. Sengstock, Nat. Phys. **8**, 71 (2012).
[30]P. A. M. Dirac, Proc. Cambridge Philos. Soc. **26**, 376 (1930).
[31]J. Frenkel, *Wave Mechanics* (Clarendon Press, Oxford, 1934).
[32]A. D. McLachlan, Mol. Phys. **8**, 39 (1964).
[33]J. Broeckhove, L. Lathouwers, E. Kesteloot, and P. Van Leuven, Chem. Phys. Lett. **149**, 547 (1988).
[34]J. Kucar, H. D. Meyer, and L. S. Cederbaum, Chem. Phys. Lett. **140**, 525 (1987).
[35]H.-D. Meyer and G. A. Worth, Theor. Chem. Acc. **109**, 251 (2003).
[36]A. Jäckle and H.-D. Meyer, J. Chem. Phys. **104**, 7974 (1996).
[37]A. Jäckle and H.-D. Meyer, J. Chem. Phys. **109**, 3772 (1998).
[38]*Applied Combinatorial Mathematics*, edited by E. F. Beckenbach (John Wiley and Sons, 1964), pp. 27–30.
[39]G. A. Worth, M. H. Beck, A. Jäckle, and H.-D. Meyer, "The MCTDH package," Version 8.2, 2000; H.-D. Meyer, Version 8.3, 2002; Version 8.4, 2007. See http://mctdh.uni-hd.de/.
[40]J. C. Light and T. Carrington, Adv. Chem. Phys. **114**, 263 (2000).
[41]A. C. Hindmarsh, "ODEPACK: A Systematized Collection of ODE Solvers," in *Scientific Computing*, edited by R. S. Stepleman *et al.* (North-Holland, Amsterdam, 1983), pp. 55–64.
[42]E. Hairer, S. P. Nørsett, and G. Wanner, *Solving Ordinary Differential Equations. I. Nonstiff Problems*, 2nd ed., Springer Series in Computational Mathematics Vol. 8 (Springer-Verlag, 1993).
[43]A. I. Streltsov, O. E. Alon, and L. S. Cederbaum, Phys. Rev. A **73**, 063626 (2006).
[44]A. Smerzi, S. Fantoni, S. Giovanazzi, and S. R. Shenoy, Phys. Rev. Lett. **79**, 4950 (1997).
[45]G. J. Milburn, J. Corney, E. M. Wright, and D. F. Walls, Phys. Rev. A **55**, 4318 (1997).
[46]E. Boukobza, M. Chuchem, D. Cohen, and A. Vardi, Phys. Rev. Lett. **102**, 180403 (2009).
[47]M. Trujillo-Martinez, A. Posazhennikova, and J. Kroha, Phys. Rev. Lett. **103**, 105302 (2009).
[48]M. Albiez, R. Gati, J. Fölling, S. Hunsmann, M. Cristiani, and M. K. Oberthaler, Phys. Rev. Lett. **95**, 010402 (2005).
[49]R. Gati, M. Albiez, J. Fölling, B. Hemmerling, and M. K. Oberthaler, Appl. Phys. B **82**, 207 (2006).
[50]R. Gati and M. K. Oberthaler, J. Phys. B **40**, R61 (2007).
[51]K. Sakmann, A. I. Streltsov, O. E. Alon, and L. S. Cederbaum, Phys. Rev. A **78**, 023615 (2008).